Multiscale Variability of Deep Convection in Relation to Large-Scale Circulation in TOGA COARE

SHUYI S. CHEN AND ROBERT A. HOUZE JR.

Department of Atmospheric Sciences, University of Washington, Seattle, Washington

BRIAN E. MAPES

Program in Atmospheric and Oceanic Sciences, University of Colorado, Boulder, Colorado

(Manuscript received 10 February 1995, in final form 28 September 1995)

ABSTRACT

Deep convection over the Indo–Pacific oceanic warm pool in the Tropical Ocean Global Atmosphere Coupled Ocean–Atmosphere Response Experiment (TOGA COARE) occurred in cloud clusters, which grouped together in regions favoring their occurrence. These large groups of cloud clusters produced large-scale regions of satellite-observed cold cloud-top temperature. This paper investigates the manner in which the cloud clusters were organized on time and space scales ranging from the seasonal mean pattern over the whole warm-pool region to the scale of individual cloud clusters and their relationship to the large-scale circulation and sea surface temperature (SST).

The dominant convective variability was associated with the intraseasonal oscillation (ISO). A large eastward propagating ensemble of cloud clusters marked the ISO's progress. The meridional structure of the ISO was strongly affected by the seasonal cycle with a southward shift from the Northern Hemisphere in October–November to the Southern Hemisphere in January–February. The SST had an intraseasonal signal in lagged quadrature with the cold cloudiness and rainfall in COARE. The SST increased (decreased) during the convectively suppressed (active) phases of the ISO. Enhanced low-level westerly winds occurred toward the later stages of the enhanced-convection periods of the ISO, though not always centered at the equator. The strongest westerlies tended to be located between two synoptic-scale cyclonic gyres, which were often not symmetric about the equator in the low-level wind field. This asymmetry in the anomalous equatorial low-level westerlies may have different implications for the oceanic response in the coupled atmosphere–ocean system than those centered on the equator. The cyclonic gyres contained highly concentrated deep convection, and, in four cases, the gyres developed into tropical cyclones.

Within the envelope marking the convectively active phase of the ISO, cloud clusters were frequently concentrated into westward-propagating disturbances with a local periodicity of ~2 days. These 2-day disturbances have been identified in earlier spectral studies and appear to be related to westward propagating inertio–gravity waves. In COARE, they typically contained numerous cloud clusters, which underwent a distinct diurnal cycle. Most of the cloud clusters embedded in the 2-day disturbances moved westward, though some were stationary, and a few moved eastward. A cloud-cluster tracking program identified groups of clusters (time clusters) that exhibited continuity in time and space. In the most convectively active period of the ISO, the tracking program identified almost the entire ISO cloud ensemble as a long-lasting, trackable superconvective system. This observation indicates the lack of a distinct scale-separation between convection and large-scale disturbances during the most intense convective periods in COARE.

1. Introduction

The Intensive Observation Period (IOP) of the Tropical Ocean Global Atmosphere Coupled Ocean–Atmosphere Response Experiment (TOGA COARE) was conducted from 1 November 1992 through 28 February 1993. The overall objective of COARE was to achieve a better understanding of the physical mechanisms for the coupling of the ocean and the atmosphere in the western Pacific warm-pool region. To describe and understand the principal processes that organize atmospheric convection in the warm-pool region was one of the specific scientific goals of COARE (Webster and Lukas 1992).

Deep convective phenomena in the warm-pool region exhibit a broad spectrum of temporal and spatial scales. The most prominent large-scale feature is the convective variability associated with the tropical intraseasonal oscillation (ISO), which has a 30–60 day timescale. The ISO may interact upscale with the El

Corresponding author address: Dr. Shuyi S. Chen, Department of Atmospheric Sciences, University of Washington, Box 351640, Seattle, WA 98195.
E-mail: chen@atmos.washington.edu

Niño Southern Oscillation (ENSO), which dominates the interannual-scale variability of the atmosphere–ocean coupled system (Lau and Shen 1988). It also interacts with smaller-scale phenomena. In this study, we use the COARE data to examine the interactions of the ISO with phenomena of smaller time and space scales.

Madden and Julian (1971, 1972, 1994) characterized the ISO as a slow eastward propagation of anomalous equatorial westerlies and easterlies in the lower and upper troposphere (e.g., 850 and 200 mb), respectively. Accompanying the eastward propagation of anomalous zonal wind is an eastward propagation of a large-scale region of anomalously frequent deep convection (e.g., Lau and Chan 1985; Knutson and Weickmann 1987; Rui and Wang 1990). The eastward propagating convective anomaly typically originates in the Indian Ocean, weakens as it moves across the maritime continent,[1] and reamplifies in the western Pacific warm-pool region. Although theories have attempted to explain the ISO in terms of mobile wave-CISK[2] (Lau et al. 1989), evaporation–wind feedback (Emanuel 1987; Neelin et al. 1987), frictional convergence in the atmospheric boundary layer (Wang 1988; Salby et al. 1994), radiative–convective interaction (Hu and Randall 1994), and convective discharge–recharge (Bladé and Hartmann 1993), the mechanisms for this phenomenon remain unverified.

The deep convection embedded in the large-scale convective anomaly associated with the ISO exhibits a rich multiscale temporal and spatial variability (Nakazawa 1988; Lau et al. 1991; Sui and Lau 1992; Hendon and Liebmann 1994). The amount of deep convection in the Tropics varies, in part, with atmospheric wave motions. Observations show various connections between convection and the easterly waves of 3–5 days (Chang 1970; Reed and Recker 1971), equatorially trapped Rossby waves (Zangvil and Yanai 1981), mixed Rossby–gravity waves (Liebmann and Hendon 1990), Kelvin waves (Wallace and Kousky 1968), and inertio–gravity waves (Takayabu 1994). Despite theoretical, observational, and modeling attempts to explain the mechanisms for the coupling of deep convection and atmospheric waves, it is still unclear whether deep convection is mainly modulated by the waves or acts as a forcing source of the waves, or if the two feedback positively to each other.

The deep convection in the ISO occurs in discrete mesoscale "cloud clusters" similar to those observed in other parts of the Tropics (e.g., Martin and Schreiner 1981). When many cloud clusters group together, the whole pattern of clusters may reflect the organizing structure of large-scale waves (Chang 1970). Nakazawa (1988) found superimposed structures in the cloud patterns in which westward-moving cloud clusters were embedded within a large-scale eastward-propagating "super cluster." Little is yet known regarding how the grouping of clusters into westward and eastward propagating envelopes is related to wave structures or other aspects of the large-scale circulation.

Sometimes the large-scale convective anomalies within the ISO are associated with intermittent, strong, low-level westerly wind anomalies in the equatorial warm-pool region where the climatological mean low-level and surface winds are weak. These wind anomalies last for a few days to 2–3 weeks and are known as "westerly wind bursts" (WWB) (Wyrtki 1975; Nitta and Motoki 1987; Murakami and Sumathipala 1989). The onset of a WWB is often coincident with the convectively active phase of the ISO over the eastern Indian Ocean and the western Pacific (Sui and Lau 1992). A long-lasting WWB in the equatorial region can lead to formation of a double-cyclone pair nearly symmetric about the equator (Keen 1987; Chen 1993). On shorter timescales (a few days or less), the WWB and associated convective activity are not as well documented. The cause of the WWB and its interactions with convection on various temporal and spatial scales are unknown.

Many previous studies of the large-scale tropical atmosphere often have described "convection" in terms of spatial and temporal patterns of average (or total) satellite-observed cloudiness. The mean cloudiness patterns obscure the fact that convection occurs in cloud clusters, that is, intermittently and on much smaller scales. Williams and Houze (1987) and Mapes and Houze (1993) examined the size distribution of cloud clusters in the tropical warm-pool region as a function of location and on various timescales, including the diurnal cycle and intraseasonal variation. They also tracked the cloud clusters in time to reveal patterns of formation, movement, merging, splitting, and dissipation. Using both infrared (IR) and visible satellite data, Machado et al. (1992) studied the spatial distribution and impact of vertical extent of cloud clusters on the size distribution over tropical Africa and the Atlantic Ocean. These techniques for studying the detailed spectrum of cloud cluster variability provide insight into the processes that lead to the mean cloudiness patterns and hence to linkage between large- and small-scale processes in the tropical climate system. In an idealized modeling study, Raymond (1994) suggested that the large-scale tropical circulation is sensitive to the fine precipitation structure of convective systems.

In this paper, we examine the distribution and variability of convection, wind, and sea surface temperature (SST) in the warm-pool region during the COARE IOP. We analyze the satellite-observed cloud data in terms of both the continuous "mean cloudiness" and discrete "cloud cluster" points of view and attempt to

[1] The term "maritime continent" refers to Indonesia and Malaysia (Ramage 1971).

[2] CISK refers to "conditional instability of the second kind" (Charney and Eliassen 1964).

show the relationship between these two perspectives. By this method, we attempt to connect the sometimes disparate "mesoscale" and "large scale" views of the convective process in the Tropics. Our analysis covers the range of time and space scales from the seasonal average fields, through intraseasonal variability, down to individual mesoscale cloud clusters. Observations concerning some planetary aspects of the COARE IOP are given in Gutzler et al. (1994). As we proceed down scale, we can see how one scale of convective activity relates to the next. The objectives of this study are 1) to describe the multiscale variability of deep convection in relation to the large-scale atmospheric circulation and SST in the warm-pool region and, by so doing, 2) to provide a large-scale context for studies concentrating on specific processes such as air–sea fluxes and mesoscale structure and organization of individual convective systems during the COARE IOP.

Section 2 includes a description of the datasets and a brief outline of the cloud cluster finding and tracking algorithms used in this study. Section 3 examines the seasonal mean patterns of deep convection, SST, and wind fields (section 3a) and how the convection underwent a slow intraseasonal variation (sections 3b and 3c). Section 3 will also review the primary characteristics of the deep convective clouds themselves: their size distribution and their diurnal variation (sections 3d and 3e). Section 4 describes the multiscale organizations of the deep convection and large-scale circulations from intraseasonal scale to mesoscale. Section 5 examines how the individual cloud clusters group together to determine the total cloudiness. Section 6 puts forward some discussions on possible mechanisms and implications of the observations and conclusions.

2. Data, methods, and definitions

a. Data sources

The primary data used in this study are hourly infrared (IR) satellite images from the Japanese Geosynchronous Meteorological Satellite (GMS) provided by the Australian Bureau of Meteorology, with about 10-km resolution (highest resolution approximately 9 km at the subsatellite point), the European Centre for Medium-Range Forecasts (ECMWF) uninitialized global wind analysis fields at 0000 and 1200 UTC, and the National Meteorological Center (NMC) analyzed monthly mean SST. These data are supplemented by sounding data from the National Center for Atmospheric Research (NCAR) integrated sounding system (ISS, Parsons et al. 1994), the TOGA Tropical Atmosphere and Ocean (TAO) buoy data (McPhaden 1993), the Microwave Sounding Unit (MSU) estimated precipitation (Spencer 1993), NOAA WP-3D aircraft lower-fuselage radar, and MIT radar on R/V *Vickers*. The observational domains of TOGA COARE

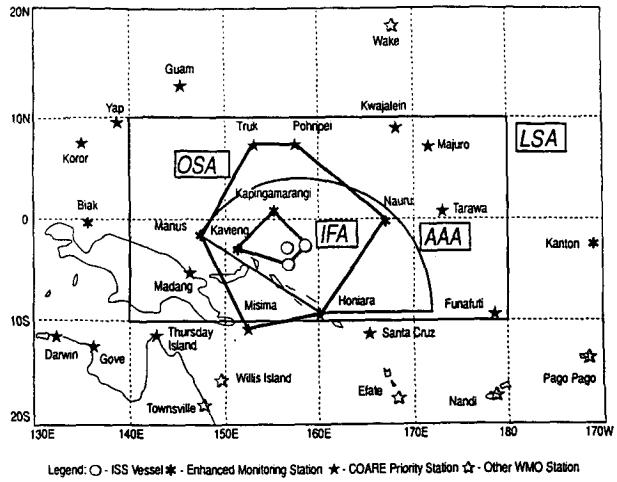

FIG. 1. Observational domains during the intensive observing period (IOP) of TOGA COARE. The large-scale domain (LSA), the outer sounding array (OSA), the aircraft accessible array (AAA), and the intensive flux array (IFA) are outlined. The key refers to the symbols used to represent the observational platforms.

are identified in Fig. 1, including the COARE LSA (large-scale array) and its subdomains OSA (outer sounding array), AAA (aircraft accessible array), and IFA (intensive flux array).

b. IR temperature threshold selection

Infrared temperature threshold selection for tropical deep convection was summarized in Mapes and Houze (1993). Machado et al. (1992) showed that, for pixel reflectivity (defined by the visible channel radiance) larger than 0.8, the cloud coverage is almost unchanged between thresholds 253 K and 230 K, which means that most of the highly reflective (optically thick) clouds selected by 253 K have tops at higher altitude (IR temperature < 230 K). In this study, we use 235 K to indicate the overall high cloudiness associated with deep convection. Arkin and Meisner (1987) have also used 235 K as the threshold IR temperature for the GOES (Geostationary Operational Environmental Satellite) precipitation index (GPI). A colder threshold of 208 K is used to characterize the very cold cloud clusters. The 208 K threshold is a closer approximation to the *boundary* of the precipitating core of tropical convective systems. The choice of 208 K, while arbitrary, is a rather conservative indicator of precipitating deep convection. For example, this definition was used to select cloud clusters for intensive sampling by radar-bearing COARE aircraft, which never failed to find a radar echo (rain) area of at least comparable size to the associated region of 208 K cloud top. The recent results of Liu et al. (1995), using data from passive microwave satellite sensors that sense precipitation more directly, indicate that ~90%–95% of <208 K patches (~3000 km^2,

the size of the SSM/I 19-GHz footprint) overlie SSM/I-derived precipitation within that SSM/I pixel. These temperature thresholds, however, are arbitrary and we do not use them to estimate precipitation amount.

c. Percent high cloudiness

We present mean cloudiness patterns in terms of the percent high cloudiness (PHC), which is the fractional coverage (in time or space) of cloud with IR temperature less than a given threshold. The daily, weekly, and monthly PHC are calculated as the percentage of images colder than the threshold temperature at each pixel. PHC_{208} and PHC_{235} will be used to denote the fractional coverage of clouds with IR temperatures of <208 K and <235 K, respectively.

d. Cloud cluster identification

We define a cloud cluster as a closed contour of a threshold IR temperature in a GMS image. An objective technique to identify and track connected cloud clusters of a specified IR temperature threshold was developed by Williams and Houze (1987) and further applied and extended by Mapes and Houze (1993). The algorithm is described in detail in those studies. To identify a cluster at a particular time, connected areas of cold cloudiness (called line clusters) are found within each line (row) of the data array containing one satellite image. The line clusters on two successive lines must share a column (not merely touch diagonally) to be considered connected. Each cloud cluster is summarized by its area and centroid position. An IR temperature threshold of 208 K defines the cloud clusters identified in this study. We used this method to identify all such cloud clusters in the field of view of the GMS and the COARE domains (Fig. 1).

e. Large-scale wind field

The twice daily (0000 and 1200 UTC) ECMWF wind analysis field is used to describe the large-scale circulation over the warm-pool region. Monthly mean and weekly mean wind fields are calculated from the ECMWF global wind analysis with $2.5° \times 2.5°$ grid resolution. Wind measurements from the soundings and TAO buoy within the OSA and IFA are used to describe large-scale conditions over the IFA.

f. Definitions of terms describing satellite-observed cloud patterns

Since we use several terms to describe the satellite-observed cloud patterns associated with deep convection, and since these terms tend to sound somewhat similar, we present the following list of definitions to aid in the discussion of results in subsequent sections of this paper. Some of these terms have already appeared, while others will be introduced later.

Cloud cluster—A cloud cluster is a region of cold cloud tops surrounded by a single closed contour of a threshold IR temperature in a GMS image. For a low threshold IR temperature, which roughly outlines a precipitation area, a cloud cluster corresponds to what is commonly called a "mesoscale convective system" (MCS, Houze 1993, 334).

Time cluster—A time cluster is a set of cloud clusters that exhibits temporal and spatial continuity across at least two frames of satellite imagery. Because cloud clusters can split and merge, a single time cluster may consist of several cloud clusters in any given frame. If the time cluster consists of a group of cloud clusters, the overall group must exhibit a specified amount of close proximity in space and continuity in time. The members of a time cluster may form, dissipate, merge, or split during the lifetime of the time cluster.

Supercluster—Nakazawa (1988) coined the term "super cluster" to describe eastward-propagating cloud ensembles with a horizontal scale of several thousand kilometers, within which are embedded westward-moving individual cloud clusters. Mapes and Houze (1993) suggested a quantitative definition of a supercluster; they defined a supercluster as a time cluster exceeding two days in duration.

Superconvective system—As will be discussed in section 5, we find that many spatially large time clusters do not last as long as two days, and are not necessarily eastward propagating. For this reason, we introduce the term of a superconvective system (SCS), defined as a time cluster whose maximum instantaneous size (possibly comprised of several cloud clusters, as noted above) exceeds a total area of 9×10^4 km^2. No minimum lifetime criterion is imposed. The lifetimes of SCSs range from several hours to a few days. The supercluster, defined above, is a special long-lived case of the more general SCS.

ISO cloud ensemble (ICE)—An ISO has a convectively active phase and a convectively suppressed phase. We call the cloud population constituting the convectively active phase of the ISO the ISO cloud ensemble (ICE).

3. Overview of deep convection, SST, and atmospheric circulation during the COARE IOP

a. Four-month mean high cloudiness, SST, and wind fields

The mean distributions of PHC, 850- and 200-mb winds, and SST over the warm-pool region during the four months of the IOP (November 1992 through February 1993) provide a background against which higher-frequency variability took place. Here we examine the mean large-scale features of these fields in the GMS domain (80°E–160°W), which spans the eastern Indian Ocean and western Pacific. Figure 2 shows the PHC_{208} and PHC_{235} for the IOP over the

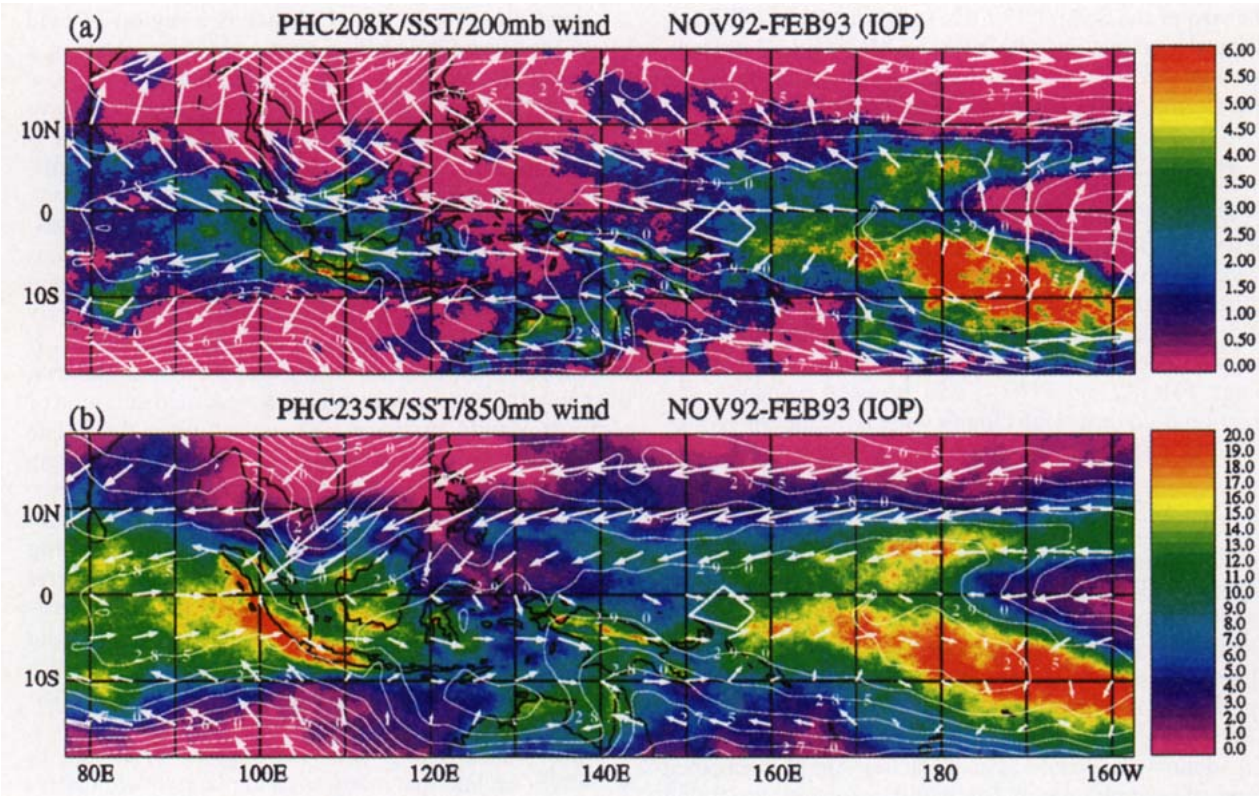

FIG. 2. The percentage of high cloudiness (PHC, the fractional time coverage of cloud with infrared temperature less than a given threshold) is overlaid with mean NMC SST analysis and the mean ECMWF global wind analysis. (a) PHC_{208} (<208 K) and wind at 200 mb and (b) PHC_{235} (<235 K) and wind at 850 mb for November 1992 through February 1993. Wind vectors are scaled such that a 10 m s^{-1} wind is represented by a vector that would be 2.5° in length on the map. The COARE IFA is outlined.

GMS domain. These satellite high-cloudiness fields are overlaid with four-month mean SST and winds at 200 and 850 mb, respectively.

The SST contours (both panels of Fig. 2) show the configuration of the warm pool during the COARE IOP. COARE followed the long-lasting 1991–1992 warm ENSO event (see *Climate Diagnostics Bulletin,* CAC/NMC/NOAA, January 1994), and the warm pool was displaced eastward from its climatological position. A broad area in the equatorial western Pacific (5°N–10°S, 150°E–180°), including the IFA and most parts of the LSA, was covered by a warm sea surface (SST $\geq$ 29.0°C). The highest SST (~29.8°C) was found far to the southeast of the COARE domain (centered at about 10°S and 175°W). A second high SST area (SST $\geq$ 29.5°C) was in the Arafura Sea, just north of the Australian continent. The equatorial cold tongue extended westward into the western Pacific from the eastern Pacific and yielded a region of strong equatorial SST gradient near the date line.

The mean 200-mb winds over the warm-pool region (Fig. 2a) were predominantly easterlies and divergent, especially in the meridional component. The mean 850-mb winds (Fig. 2b) featured strong easterlies north of the equator, weak westerlies at the equator, and stronger westerlies 5° south of the equator. This pattern predominated throughout most of the GMS domain, except in the central Pacific where easterlies prevailed on both sides of the equator. The mean low-level zonal winds in the COARE inner domains (IFA and OSA in Fig. 1) were westerly. The South Pacific convergence zone (SPCZ) was well defined around 5°S, 170°W, where it was collocated with the highest SST area. Relatively weak cross-equatorial flow from the Northern Hemisphere between 120° and 150°E marked an equatorial trough that persisted throughout the IOP. Mean low-level convergence of the meridional wind component occurred at about 5°S at the COARE longitudes. The COARE inner domains were located in this weak meridional convergence zone.

The highest PHC (Fig. 2) occurred in the SPCZ, where mean low-level convergence and the highest SST were collocated during the Austral summer. The deep convection in the intertropical convergence zone (ITCZ), with its local maximum PHC between 5° and 10°N near the date line, was much less intense than the SPCZ during the IOP. Another persistent convective region was tied to the west coast of Sumatra and Java (7°S, 105°E). The four-month mean high cloudiness in the Australian summer monsoon region, extending

eastward from 125°E across north Australia and the Gulf of Carpenteria, was much less than that in the SPCZ because of the relatively transient nature of the monsoon circulation. The COARE inner domains were located in a region with moderate mean high cloudiness, which decreased to the west and increased to the east. The total high cloudiness (as measured by PHC_{235}, Fig. 2b) was about 10%–15% over the IFA and 15%–20% over the eastern portion of the LSA. Regions with moderately cold cloud tops (208–235 K) were closely related to deep convective clouds, as is apparent from the fact that the PHC_{235} and PHC_{208} centers were collocated, with the moderately cold clouds generally spread over a larger area.

b. *Intraseasonal variation of high cloudiness and wind*

Figure 3 shows time–longitude sections of daily PHC_{235} and 850-mb zonal wind across the GMS domain (80°E–160°W). It covers the time period October 1992–February 1993, which includes the COARE IOP plus the preceding month. The 10-km pixel values of daily PHC_{235} (Fig. 3a) are averaged over 0.5° × 0.5° grid elements. The shading denotes the number of grid elements between 20°S and 20°N, with daily PHC_{235} > 25%. It emphasizes deep convective episodes that extended over a wide meridional extent and persisted longer than 6 h. The daily zonal component of the 850-mb wind in Fig. 3b is averaged over the latitude band 5°N–5°S.

The most prominent features are three large-scale episodes of enhanced convective activity (Fig. 3a) and anomalous westerlies (Fig. 3b). These events reflect the ISO propagating eastward across the GMS domain. We refer to them as ISO1, ISO2, and ISO3 (Fig. 3a), according to the sequence of their appearance. We refer to the large-scale cloud ensemble associated with each of the intraseasonal disturbances as an ISO cloud ensemble (ICE, see definition in section 2f). We refer to the enhanced westerlies associated with ISO2 and ISO3 as WWB2 and WWB3, respectively (Fig. 3b).

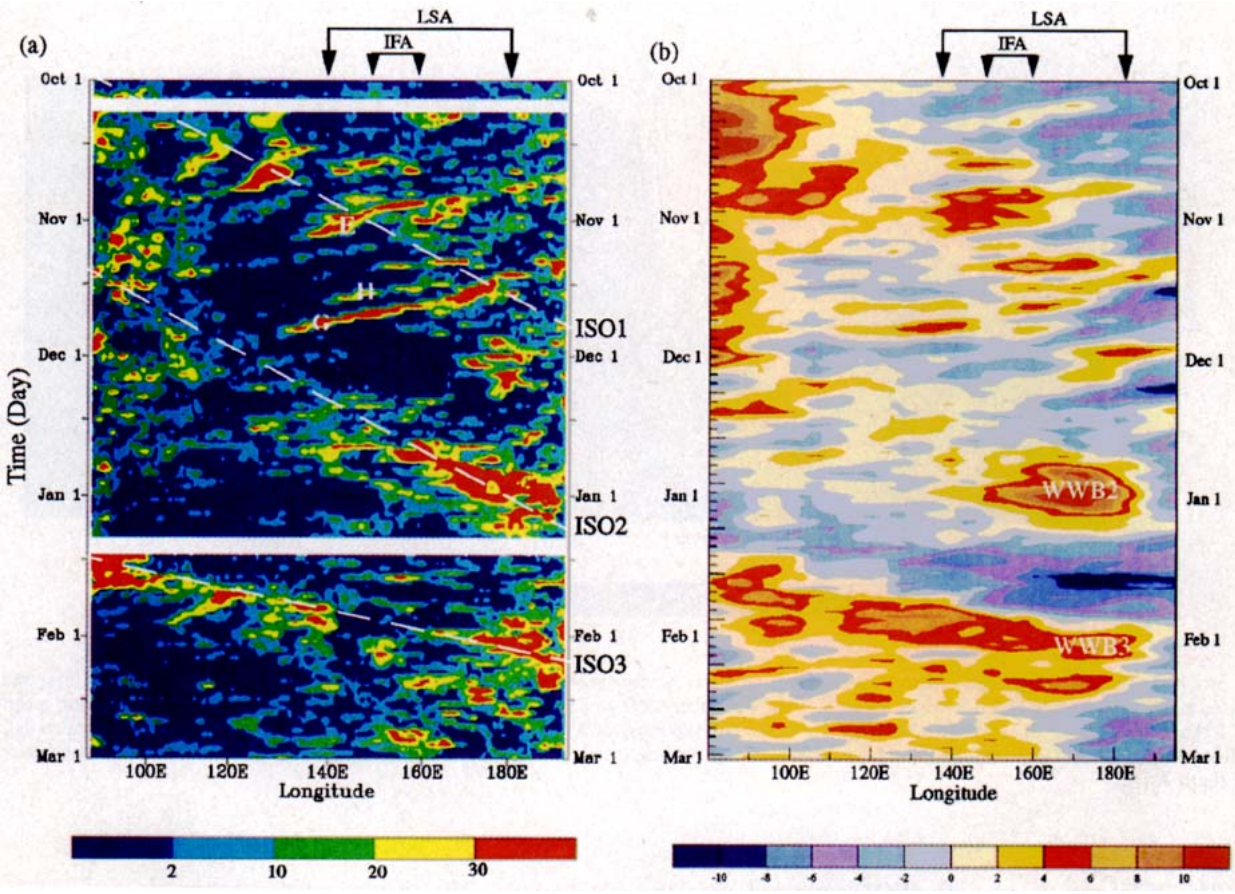

FIG. 3. (a) Time–longitude section of daily PHC_{235} index. Each one day by 0.5° longitude grid element is color coded according to the value of the PHC_{235} index, which is the meridional summation of the number of daily PHC_{235} > 25% between 20°S and 20°N. The three tropical cyclones (Elsie, Gay, and Hunt) are marked as E, G, and H. Long dashed lines indicate tracks of three events of ISO. (b) Time–longitude section of daily ECMWF 850-mb zonal wind component (m s^{-1}) averaged between 5°N and °S. The enhanced westerlies associated with ISO2 and ISO3 are denoted as WWB2 and WWB3, respectively. Locations of the LSA and IFA are indicated at the top of the figures.

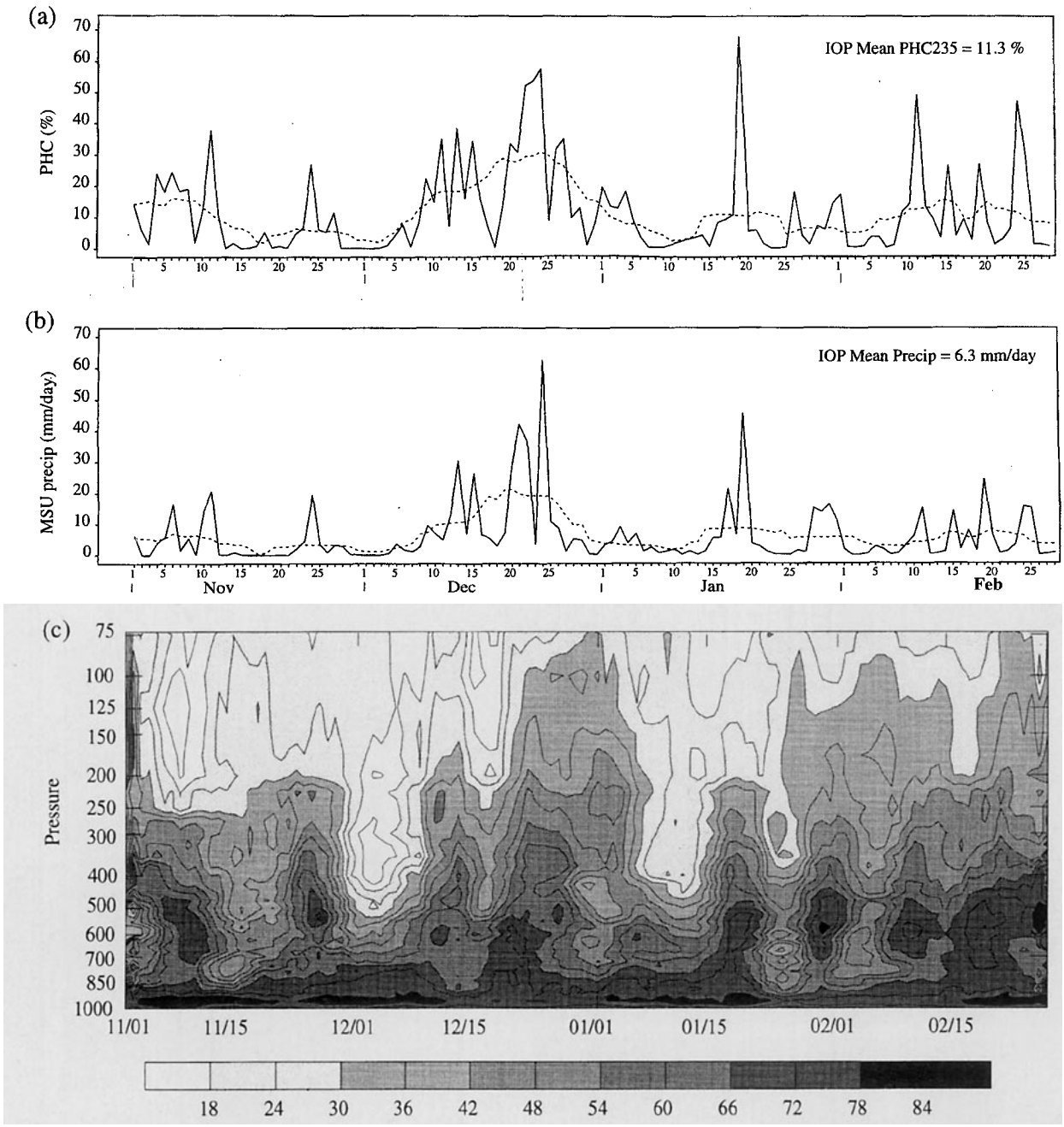

FIG. 4. Time series of (a) daily PHC_{235} (solid line) and 5-day running mean (dashed line) and (b) daily MSU precipitation (solid line) and 5-day running mean (dashed line) over the IFA from November 1992 to February 1993. (c)–(d) Time–height plot of 5-day running mean of RH and zonal wind (m s^{-1}) from soundings within the IFA [courtesy of X. Lin and R. H. Johnson, see Lin and Johnson (1996) for details]. (e)–(g) The surface RH, u, and SST (daily: solid line, 5-day running mean: dashed line) from the TAO buoy at (2°S, 156°E) near the center of the IFA.

The ICE associated with ISO1 appeared near the western boundary of the GMS domain (west of 100°E) in early October and propagated eastward at an average speed of ~4 m s^{-1} (Fig. 3a). Its eastward speed slowed to ~1 m s^{-1} east of ~150°–160°E at the beginning of November. The change in the eastward propagating phase speed of large-scale convective anomalies associated with the ISO has also been noted by Gutzler et al. (1994). In mid-November, the second ICE began to propagate eastward from the eastern Indian Ocean

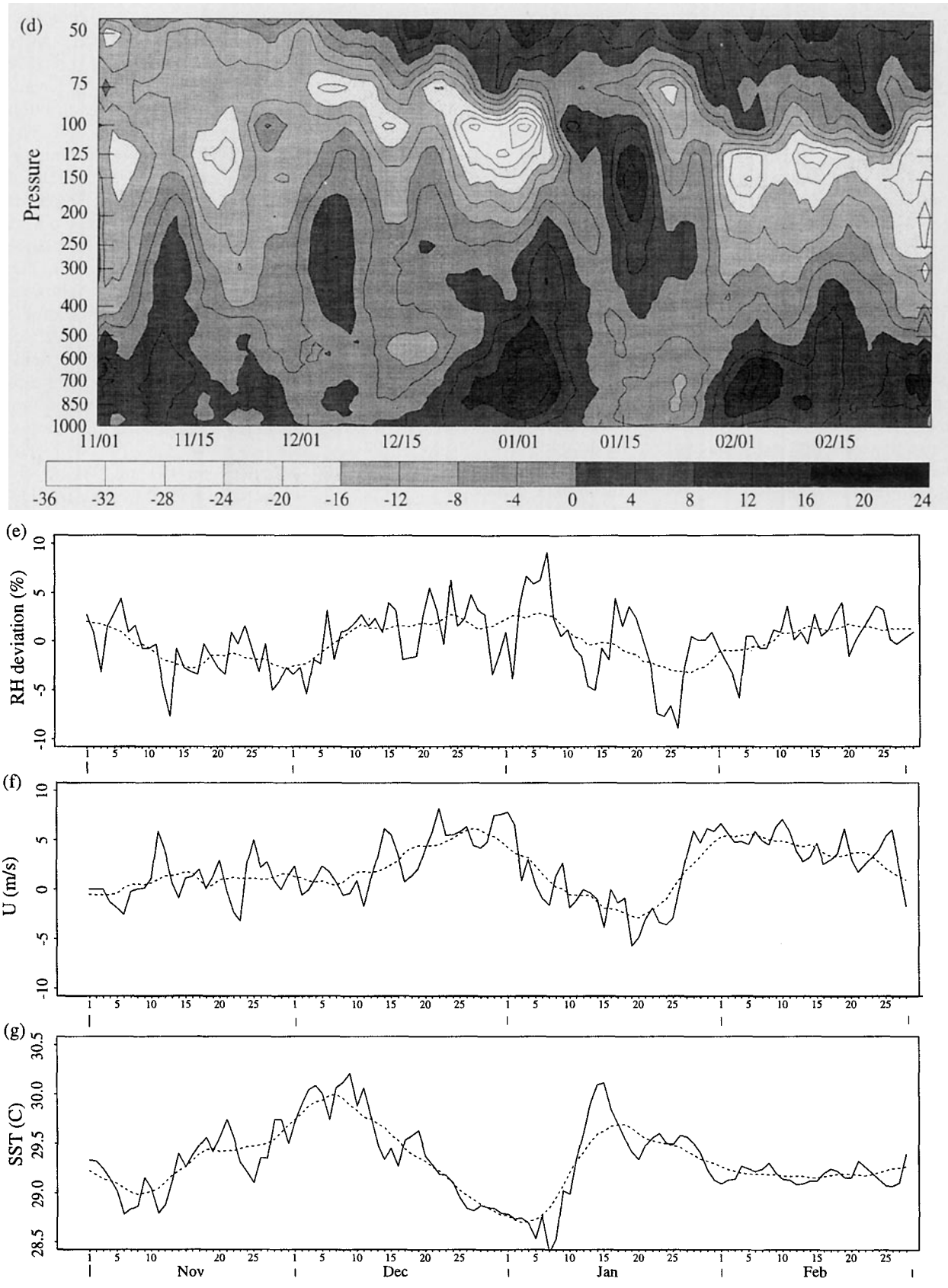

FIG. 4. (*Continued*)

at an average phase speed of ~4.5 m s^{-1}. Convection was very active over the COARE region (140°E–180°) between mid-December and the beginning of January. Shortly after this time (about 20 January), the third ICE appeared over the eastern Indian Ocean, while the anomalous convection declined over the western and central Pacific. ISO3 propagated eastward slightly faster than ISO2 at ~6.5 m s^{-1} (Fig. 3a) and passed through the COARE region in late January to early February. Both ISO2 and ISO3 produced westerly wind bursts over the western Pacific (WWB2 and WWB3 in Fig. 3b).

Just as remarkable as the eastward propagating active convective episodes are the eastward propagating suppressed cloudiness episodes, which are identifiable in Fig. 3a as the areas with very low PHC_{235}. Such suppressed episodes, accompanied by anomalous easterlies (Fig. 3b), passed through the COARE domain twice during the IOP. The first passage was from mid-November through early December, the second from mid- to late January. During these two suppressed periods, very few intense, long-lasting mesoscale convective systems occurred in the COARE domain. The physical relationship of the anomalous low-level easterly wind to the suppression of the deep convection remains unclear.

Another conspicuous feature of Fig. 3a is that westward propagating synoptic-scale convective disturbances were superimposed on the large-scale eastward propagating signals of active convection. The most noticeable are three tropical cyclones (Elsie, Gay, and Hunt), which all formed in the Northern Hemispheric part of the LSA in the wake of ISO1 (E, G, and H in Fig. 3a).

c. *Time series over the IFA*

The intraseasonal variation of cloudiness and wind seen in Fig. 3 provides a large-scale context in which to view the time series of conditions in the IFA, which was the center of operations in the COARE IOP (Fig. 1). Figure 4 shows time series of cloudiness, rain, wind, SST, and humidity in the region of the IFA. Five-day running means of PHC_{235} (Fig. 4a), MSU-derived precipitation (Fig. 4b), tropospheric RH and zonal wind component u (Figs. 4c and 4d, see Lin and Johnson 1996), and TAO surface RH, zonal wind, and SST (Figs. 4e, 4f, and 4g) all show the three active phases of ISO1, 2, and 3 (seen in Fig. 3a), as well as the two intervening suppressed phases. The GMS IR high cloudiness and MSU-derived precipitation (two independent measurements) are consistent in the timing and intensity of convective events over the IFA.

The IOP began at the time of the active phase of ISO1 over the COARE domain (early to mid-November in Fig. 3). From 13 November to 8 December, the IFA was in the suppressed phase of the ISO. The deep convective activity started to increase over the IFA on 9 December, and four successive large convective systems developed within or near the IFA (Fig. 4a). After a short break period from 17–19 December, the IFA returned to a much more continuous intensive convective period, which lasted from 20 December through the first few days of January (Figs. 4a and 4b). The suppressed phase of ISO2 lasted from 6 to 26 January. The convective events in mid-January were not related to the ISO, as will be discussed in section 4c. The onset of the convectively active phase of ISO3 was not as clearly defined over the IFA as the previous one, since the third ICE "jumped" over the IFA (Fig. 3a). The ISO3 active phase lasted through most of February. However, as we will see in section 4b, most of the convective activity was east and south of the IFA.

The upper-tropospheric and surface humidity fields showed a consistent intraseasonal variation in the 5-day running means (Figs. 4c and 4e). During the first suppressed phase, an upper-tropospheric dry tongue (above 700 mb) dominated the IFA (Fig. 4c). The lower-tropospheric RH (between 950 and 700 mb) increased slowly from late November through early December. This increase of RH in the lower troposphere preceded the beginning of the transition period in deep convection (early to mid-December) before the onset of the active phase of ISO2. The upper-tropospheric moisture increased rapidly as soon as the first few convective systems broke out during the transition period (9–16 December). The upper-level RH peaks coincided with the deep convection and precipitation over the IFA (Figs. 4a–c). As in the case of PHC_{235} and MSU-derived precipitation, the signal of RH for the ISO3 transition–onset period in late January is not very clear in the IFA.

The vertical cross section of zonal wind (Fig. 4d) indicates three persistent low-level westerly periods associated with the three convectively active phases of the ISO. ISO2 was the only nearly complete cycle captured over the IFA. The WWB2 first appeared near the surface from 11 to 16 December, which is shown in both the TAO buoy and the sounding data (Figs. 4d and 4f). Although the 5-day running means show a continuous increase of low-level westerly wind, the surface westerlies measured on the TAO buoy were fluctuating and dropped back to less than 1–2 m s^{-1} from 17–19 December, while the PHC_{235} indicated a short break in convection. The westerlies gradually extended into a deep layer (from surface to near 200 mb) and reached a maximum intensity at 850 mb around 1 January. The upper-level easterlies began to intensify at the same time as the low-level westerlies. The peaks of the 850-mb westerlies and the 100-mb easterlies lagged behind the most intense convection and precipitation over the IFA by several days. In January, during the suppressed phase of the ISO, the IFA was characterized by anomalously strong low-level easterlies and upper-level westerlies.

The SST during the COARE IOP (Fig. 4g) is in lagged quadrature with the high cloudiness and rainfall (Figs. 4a and 4b). The SST increased (decreased) during the convectively suppressed (active) phases of the ISO. Although the result shown here is from a single TAO buoy in the IFA, observations from other buoys in the western Pacific are consistent (Zhang 1996). The relatively low SST in the active phase of the ISO is partly due to the reduced incoming solar radiation, enhanced evaporation and mixing, and deposition of cold fresh water at the ocean surface by deep convection.

The intraseasonal variation can also be found in the Convective Available Potential Energy (CAPE) calculated from the COARE sounding data. During the suppressed phases of the ISO, the boundary-layer integrated CAPE in the IFA was generally ~500 J kg^{-1} higher than in the convectively active phases (Brown 1994). An increase of CAPE with time (change in CAPE up to 1000 J kg^{-1} or more) was also found during the suppressed phases in several ISS sites over the COARE LSA (David Parsons, personal communication, 1995).

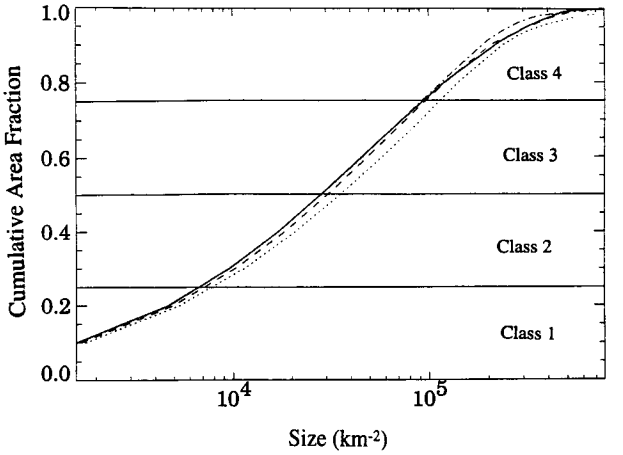

FIG. 5. Cumulative size distributions of 208 K cloud clusters. Fraction of the total sampled cloud area that is accounted for by the 208 K cloud clusters up to the indicated size for 1986–1987 (dotted line), 1987–1988 (dashed line), 1988–1989 (dot–dashed line), and 1992–1993 (solid line). The thin horizontal lines divide the size distribution into size quartiles, each quartile contributing an equal amount to the total area of cloud top colder than 208 K.

d. Size distribution of cloud clusters

The representation of high cloudiness as PHC (Figs. 2, 3a, 4a) is a good way to indicate the overall *amount* of cloudiness in a given area and/or time period. However it does not indicate *how the cloudiness arose.* For this purpose, one must delineate and characterize the phenomena producing the cloudiness. Most of the high cloudiness in the COARE region is produced by discrete mesoscale convective systems, which we represent as cloud clusters (defined in section 2f). The ensemble properties of the cloud clusters are thus an important element of a complete climatology of tropical convection.

Figure 5 shows the cumulative fraction of the total sampled cloud area in the GMS domain accounted for by the 208 K cloud clusters up to the indicated size for 1986–1987 (dotted line), 1987–1988 (dashed line), 1988–1989 (dot–dashed line), and 1992–1993 (solid line). The thin horizontal lines divide the size distribution into size quartiles, each quartile contributing an equal amount (25%) to the total area of cloud top colder than 208 K. The overall size distribution of the cloud clusters for the IOP is similar to the previous 3-yr climatology of Mapes and Houze (1993). The boundaries for the quartiles are class 1 (<6800 km^2 in area or < ~80 km in dimension), class 2 (6800–28 300 km^2 or ~80–170 km), class 3 (28 300–92 800 km^2 or ~170–300 km), and class 4 (>92 800 km^2, or > ~300 km). Previous studies of tropical cloud clusters (Williams and Houze 1987; Machado et al. 1992; Mapes and Houze 1993) show that cluster sizes are nearly lognormally distributed but deviate from the lognormality in both the smallest and largest ends of the distribution.

The population of cloud clusters in the three COARE domains (IFA, AAA, and LSA in Fig. 1) is shown in time series in Fig. 6. Each dot represents an occurrence of a cloud cluster with a specific size, expressed as equivalent radius $R_e = (A/\pi)^{1/2}$, where A is the cluster area on an hourly GMS IR image. Horizontal lines mark the boundaries of the size class quartiles defined by Fig. 5, which are slightly different than the classification used for the COARE IOP aircraft missions (Chen et al. 1995). The small class 1 cloud systems were present on more than 80% of the IOP days in the IFA (Fig. 6a), whereas class 4 systems occurred within the IFA on only ~10% of the IOP days.

The different large-scale regimes, including two suppressed phases (from mid-November to early December and mid-January) and two active phases (mid-December to early January and February) of deep convection associated with the ISO, are apparent in the total number of cloud clusters shown in Fig. 6. This variation is much more pronounced in the larger clusters than the smaller clusters. Most of the very large clusters were found *only* during the active phases of the ISO. The cloud population in other years has a similar behavior (Mapes and Houze 1993).

e. The diurnal variation of cloudiness

Figure 7 shows the diurnal cycle of area covered by <208 K cloudiness during the COARE IOP in a region bounded by 10°N–10°S, 152°E–180° subdivided according to cloud cluster size. This domain avoids the large islands so that the diurnal cycle in Fig. 7 comes primarily from oceanic cloud clusters. The diurnal cycle of the total area of cold cloud coverage is stratified

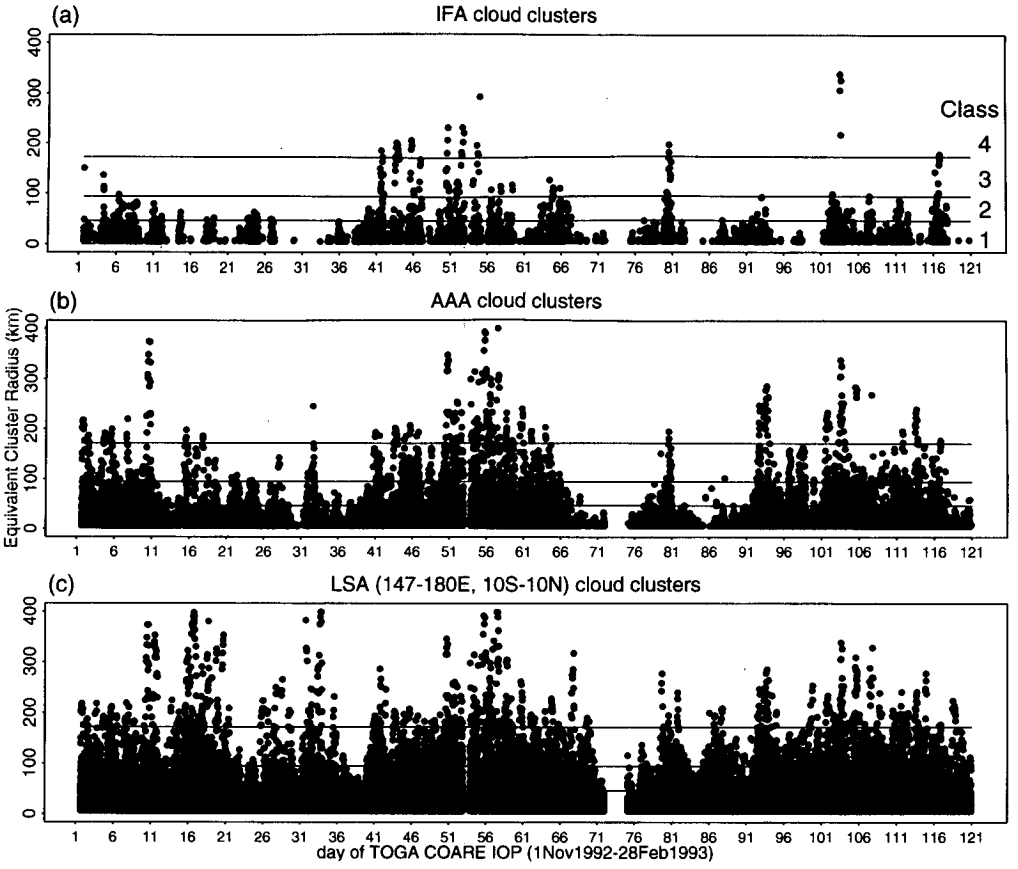

FIG. 6. Time series of occurrence of cloud clusters (closed contours of infrared temperature 208 K) as a function of their size (11–14 January missing data). Horizontal lines are boundaries of size classes 1–4 indicated in Fig. 5. Here (a), (b), and (c) refer to clusters in the IFA, AAA, and LSA shown in Fig. 1.

in Fig. 7 according to the four cluster-size quartiles (Fig. 5). This stratification shows that the diurnal cycle of the cloud clusters in the COARE IOP was size dependent. The amplitude of diurnal variation increases with the size of each cluster quartile. The area covered by the smallest clusters (class 1) had a very small amplitude of diurnal variation, while the largest clusters had a strong diurnal variation with a peak in the early morning hours and a minimum in the afternoon. The amplitude (dawn to dusk ratio) was nearly 10:1, somewhat larger than that found in the Mapes and Houze (1993) study. The diurnal behavior of these large convective systems will be discussed in section 5.

4. ISO and 2-day disturbances as revealed by total high cloudiness in relation to the large-scale wind field

a. Multiscale approach

Figures 3, 4, and 6 showed that the ISO dominated the atmospheric variability over the warm pool during the COARE IOP. Three enhanced-cloudiness phases were separated by two suppressed-cloudiness phases (Fig. 3a). The wind varied in conjunction with the convectively active and suppressed phases of the ISO (Figs. 3b, 4d, and 4f), with westerly wind bursts (WWB2 and 3) occurring in connection with ISO2 and 3. In this section, we examine more closely how the *total* cloudiness (e.g., as represented by PHC) related to variations in the large-scale wind field during each of the ISO events by proceeding down scales in both time and space.

We will first break the IOP mean cloud pattern of Fig. 2 down into weekly segments to see how the geographic structures of overall cloudiness and wind over the entire tropical Indo–Pacific region change as the ISO proceeds (section 4b). In section 4c, we will present high-resolution time–longitude sections of total high cloudiness and wind data to emphasize synoptic-scale and mesoscale features that are filtered out in the weekly patterns. In section 5, we will break the total (mean) cloudiness patterns down into individual cloud clusters to investigate how the clusters group together in time and space to make up the large-scale cloud patterns. By focusing on successively smaller time and

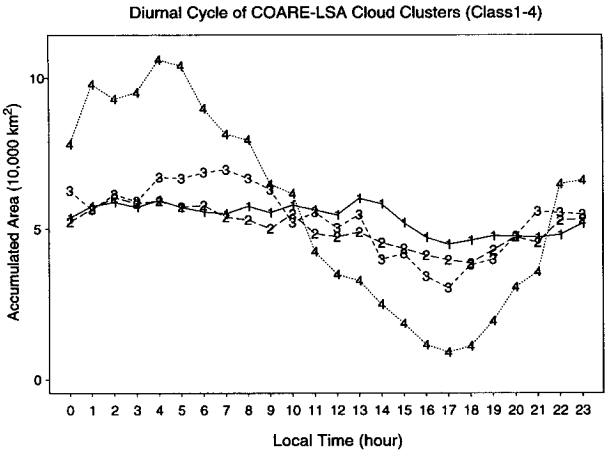

FIG. 7. Diurnal cycle of the accumulated cloudy area covered by the 208 K cloud clusters over the domain of 10°N–10°S, 152°E–180° for each of the four size classes.

space scales in these following discussions, we show how deep convective activity in the Tropics is the product of coherent group variability of smaller-scale convective systems.

b. *Weekly high cloudiness and wind: Horizontal structure of the ISO*

Figure 8 shows weekly maps of PHC_{235} and mean ECMWF wind analysis at 850 mb. These maps emphasize the horizontal variability of deep convection and large-scale circulation during COARE. In addition to the zonal propagation of the ISO seen in the time–longitude plots (Fig. 3), the weekly maps show the meridional structure of the ISO and other large-scale disturbances. Tropical cyclones and other large-scale vortices, the Australian monsoon, and westerly wind bursts are all more clearly described by the weekly maps. The mean central locations of the three ISO cloud ensembles are marked as ICE1, 2, and 3 on the weekly maps in Fig. 8. Features evident in Fig. 8 but not seen in the four-month mean fields of PHC and wind of Fig. 2 or in the time–longitude format of Fig. 3 are as follows.

1) The seasonal cycle strongly affected the meridional structure of the ISO. The maximum PHC and strongest westerlies migrated from the Northern Hemisphere in October–November (Figs. 8a–f) to the Southern Hemisphere in January–February (Figs. 8k–s). ICE1 was north of the equator (0°–10°N, in Figs. 8a–d). ICE2 and ICE3 gradually shifted to south of the equator (5°–10°S, Figs. 8h–p) during the Austral summer. Hendon and Salby (1994) and Takayabu (1994) noted a similar southward seasonal shift in other years.

2) The ICE interacted with the ITCZ and the SPCZ. Convection was active in the ITCZ near the dateline during the suppressed phases of the ISO over the western and central Pacific region (Figs. 8a, 8f, 8m–o) and was suppressed during the active phase of each ISO (Figs. 8c, 8i–j, and 8q). The ITCZ and the SPCZ tend to reestablish quickly after the ICE has diminished.

3) Westerly wind bursts during COARE had a wide range of spatial and temporal scales and were not always associated with the ISO. Murakami and Sumathipala (1989) and Sui and Lau (1992) showed that the WWBs can vary from several days to several weeks. COARE included events lasting from one week (150°–170°E in Fig. 8d and 170°E–180° in Fig. 8g) to almost three weeks (Figs. 8j–l and 8p–r). Although the physical nature of interaction between WWBs and deep convection on these spatial and temporal scales is the subject of debate, the collocations of the two are evident.

4) Rossby-wave-like disturbances (double cyclonic gyres straddling a belt of strong westerlies) were evident in all three events of ISO but not necessarily centered on the equator. Such cyclonic gyres occurred both over the eastern Indian Ocean (80°–90°E, in Figs. 8f, 8m, and 8n) and the western Pacific (Figs. 8g, 8j, 8k, and 8s). The high cloudiness tended to be strongly enhanced in the gyres and in the enhanced westerlies lying between the gyres. In a numerical modeling study, Lau et al. (1989) suggested that a cyclonic vortex pair straddling the equator is associated with the Rossby modes generated at the development stage of the Kelvin mode disturbances. Previous observations show that the cyclonic gyres can develop into double-cyclone pairs on both sides of the equator when the WWB and the gyres are nearly symmetric about the equator (Keen 1987; Chen 1993). During COARE, the cyclonic gyres were often not symmetric about the equator (e.g., Figs. 8k and 8s), and COARE contained no examples of double-cyclone pairs. In fact, the observed WWBs and the most intense convection in COARE were usually not symmetric about the equator, suggesting substantial non-Kelvin components. This asymmetry of WWB can also induce a rather different oceanic dynamical response than those centered on the equator.

5) The development of tropical cyclones Elsie, Gay, Hunt, and Kina were closely related to near-equatorial westerlies and their associated gyres. WWB1 (150°E, Fig. 8b), associated with the ISO1, was centered slightly north of the equator. The cyclonic gyre north of the westerlies became cyclone Elsie (Figs. 8b and 8c). The twice daily ECMWF wind analyses reveal that the near-equatorial westerlies associated with Elsie were a precursor to a short period WWB over the COARE LSA (Fig. 8d). This relatively short-lived WWB and associated cyclonic circulation north of the westerlies spawned the tropical cyclones Gay and Hunt (~150°–170°E, Fig. 8e). WWB2 (160°E in Fig. 8j), associated with the ISO2, was centered at 3°S. As a result, in this case, the Southern Hemisphere cyclonic

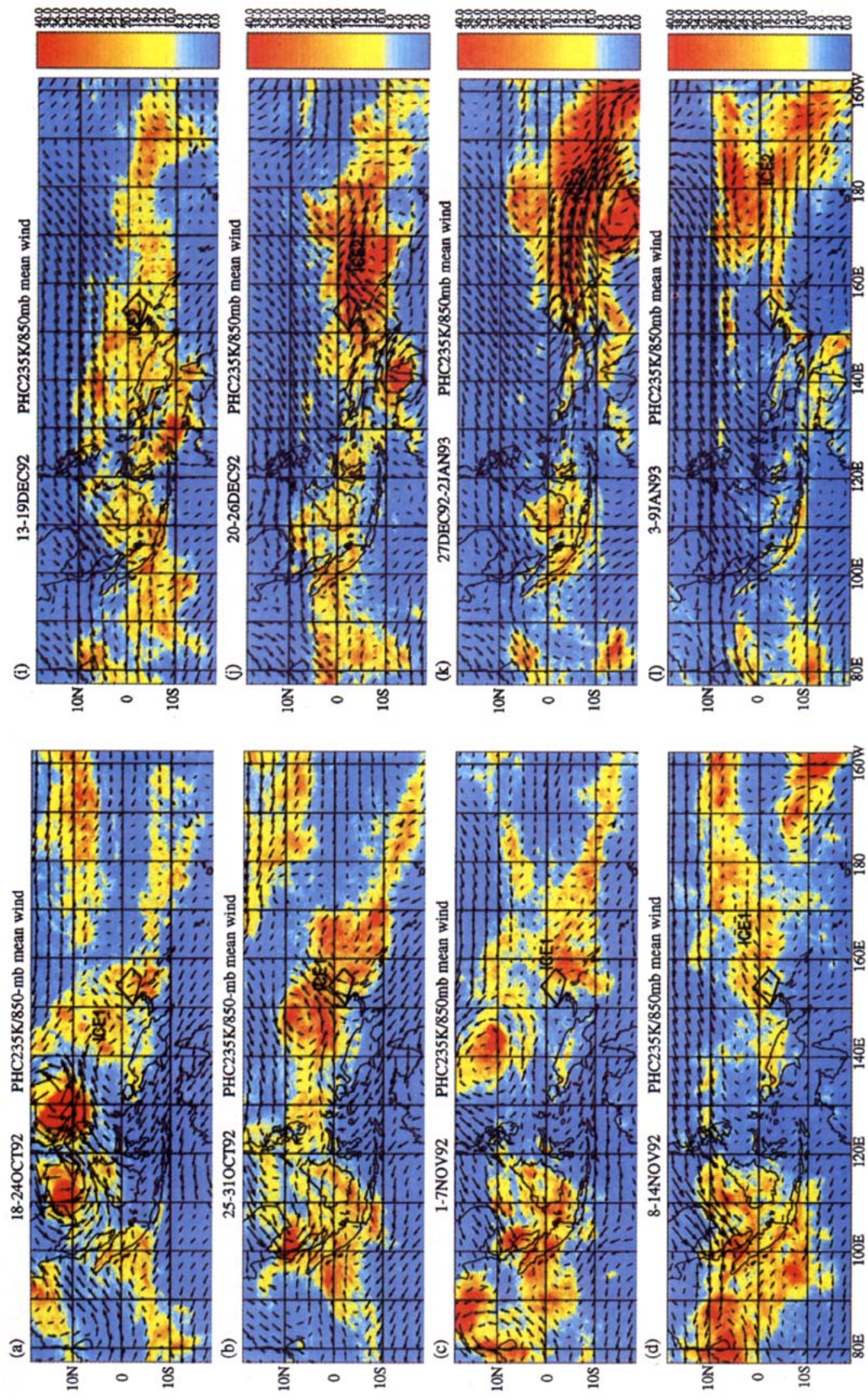

FIG. 8. Weekly percent high cloudiness (PHC), calculated as the percentage of time during the week that each 10 km × 10 km pixel in the GMS IR image had a value of 235 K or less, for each of the 18 weeks from 18 October 1992–27 February 1993. Also shown is the weekly mean wind from the ECMWF global wind analysis at 850 mb with 2.5° × 2.5° grid resolution. Wind vectors are scaled such that a 20 m s^{-1} wind is represented by a vector that would be 2.5° in length on the map. The COARE IFA is outlined. The mean central locations of the three ISO cloud ensembles are marked as ICE1, 2, and 3.

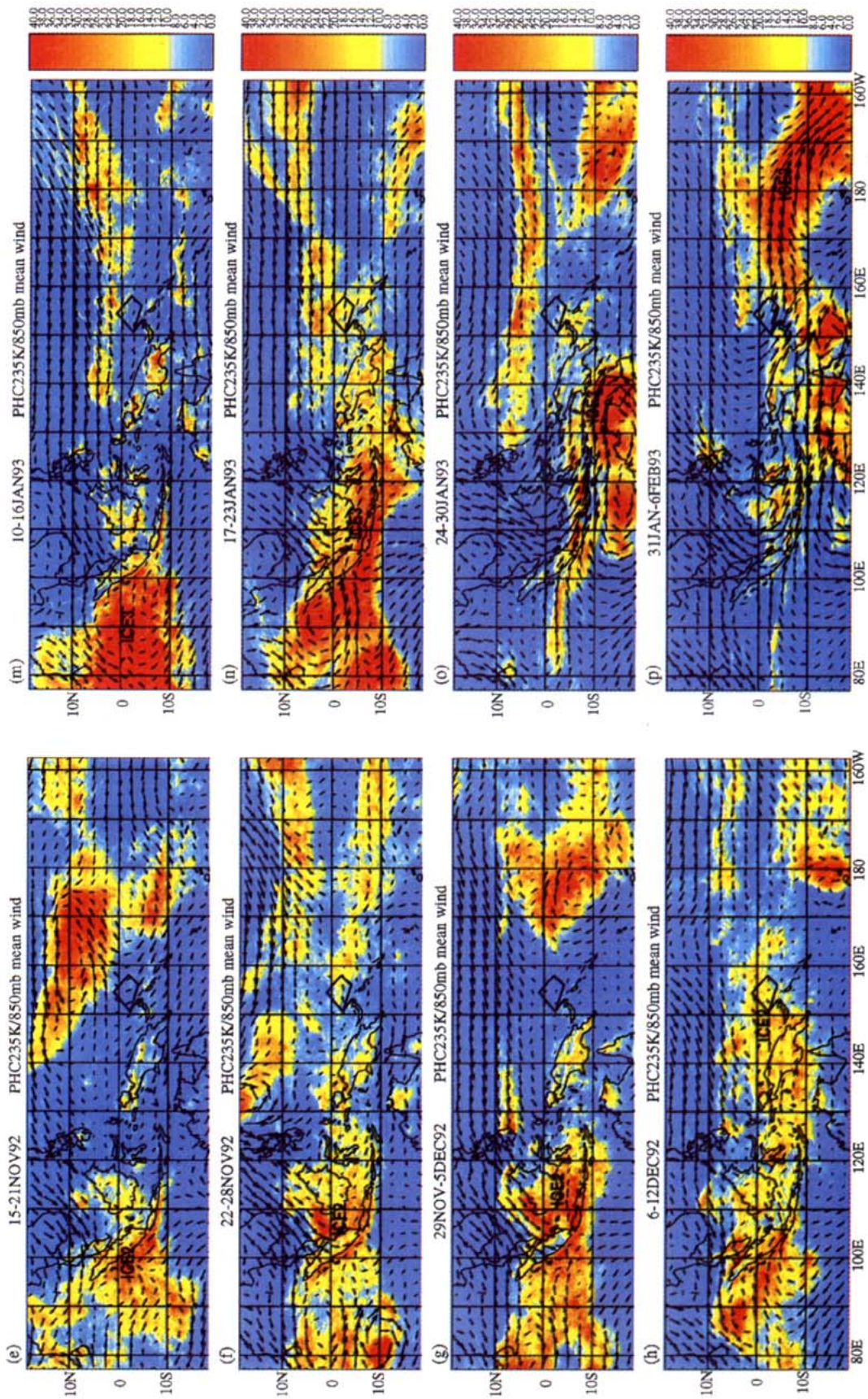

FIG. 8. *(Continued)*

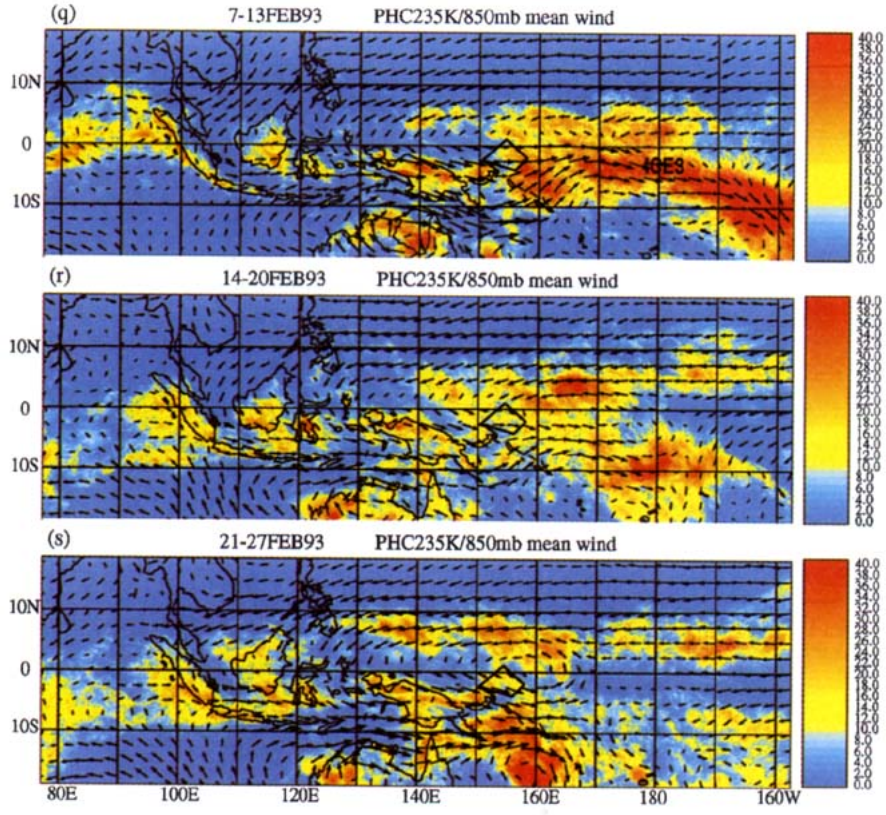

FIG. 8. (*Continued*)

circulation developed into tropical cyclone Kina on 28 December 1992 (12°S, 170°E; see Fig. 8k).

6) The ICEs were strongest over open oceans, specifically in the eastern Indian and western Pacific Oceans, and they were considerably weaker over the islands and peninsulas of the maritime continent (centered ~115°E). The reduction in convective intensity of the ISO over the maritime continent sometimes leads to the impression of a sudden jump in its eastward progression from the eastern Indian Ocean (e.g., Figs. 8m and 8n) to the western Pacific (Figs. 8p and 8q).

7) Active deep convection occurred much more frequently in low-level near-equatorial westerlies than easterlies, except within the ITCZ (5°–10°N), over the western and central Pacific. The largest and most intense ICEs in the COARE LSA were all found in low-level westerlies (e.g., Figs. 8d, 8g, 8j, 8k, 8p, and 8q). In contrast, when the equatorial wind field was predominantly easterly, especially over the eastern part of the COARE LSA, deep convection was infrequent or nearly absent (e.g., Figs. 8b, 8h, 8m, and 8n). Such suppression in easterly winds mostly occurs downstream of the central Pacific SST cold tongue (Fig. 2). Advection of the relatively cool and dry (low moist static energy) air from the eastern central Pacific and/or low-level divergence associated with the equatorial easterlies evidently suppresses convection.

8) Strong northeasterlies over the South China Sea can penetrate into the equatorial region and turn into northwesterlies after crossing the equator. Strong cross-equatorial flows over the South China Sea are often associated with "cold surges" from the Asian continent (Lau 1982; Chang and Lum 1985). During the COARE IOP, cold surges sometimes, but not always, preceded the onset of equatorial westerly wind bursts (e.g., Figs. 8n–8p). Some studies (e.g., Lau 1982) have argued that these northerly flows may suppress convection north of the equator but promote it further downstream. Cold-surge flows may somehow have been responsible for the suppressed area extending southeastward from the South China Sea into the equatorial region 120°–130°E, seen in the four-month mean map (Fig. 2). However, systematic interaction of the cold surges, ICEs, and WWBs is not obvious when viewing the weekly maps in Fig. 8.

9) The passage of ISO3 appears to have triggered the onset of the Australian summer monsoon. Figures 8m–8p show that the January active period of the Australian monsoon, as evidenced by high cloudiness and cyclonic circulation, began immediately after the approach of the eastward propagating ISO3. Hendon and Liebmann (1990) also found, from a 30-yr wind and rainfall record for Darwin, that the onset of the Australian monsoon typically coincides with the arrival of

eastward-propagating convective and zonal wind anomalies.

c. *Synoptic-scale and mesoscale features*

To reveal *synoptic-scale* (one to several days) and *mesoscale* (a few hours to a day) variability, Fig. 9 shows high-resolution time–longitude sections of total high cloudiness and 850-mb wind. At each time and longitude, the color indicates the fraction of a 10° latitude band (5°N–5°S for November; 0°–10°S for December, January, and February) that was covered by cloudiness with IR temperature less than 208 K. The wind vectors are the daily (average of 0000 and 1200 UTC) ECMWF wind analysis at 850 mb averaged over the same 10° latitude band.

In November (Fig. 9a), the deep convection was relatively active in the wake of ISO1 earlier (also see Figs. 8c and 8d) and became suppressed over the LSA in the second half of the month (Figs. 8e–g). The subsequent development of two large convective systems during 10–11 November (Fig. 9a) coincided with a ~5-day period of strong surface-to-midtropospheric westerly wind seen in Figs. 4d and 4f. The maximum meridionally averaged westerly wind at 850 mb was 20 m s^{-1} (Fig. 9a), while the actual local wind measured by the ISS site in Nauru (~165°E) reached over 30 m s^{-1}. Inspection of the twice daily ECMWF wind analysis (not shown) indicates that this relatively short WWB may have been related to tropical cyclone Elsie (Figs. 8b and 8c). The IFA and OSA (150°–165°E) were relatively suppressed from 13 November to 9 December (Figs. 9a and 9b), except for isolated deep convective clouds and a few relatively short-lived mesoscale convective systems in late November.

In the COARE IFA longitude, December (Fig. 9b) brought a striking transition from a period of substantially suppressed convection to some of the most active convection in COARE. During the suppressed phase of ISO2 (mid-November to 9 December), the low-level wind was generally weak over most of the LSA (140°–180°E). Starting 8–10 December, moderate westerlies associated with the eastward propagating ICE2 approached the IFA from the west, while strong low-level easterlies developed east of the IFA. The suppressed period in the IFA was interrupted on 10 December by four westward-propagating groups of cloud clusters across the longitude of the IFA during 10–16 December. Meanwhile, low-level westerlies started to increase to the west of the IFA (Fig. 9b).

A seemingly sudden onset of convective activity and strengthening westerlies near 140°–170°E is seen on 20 December. Throughout the period 20–31 December, the westerlies strengthened and extended eastward as ICE2 slowly propagated eastward. At the end of the month, the westerlies spanned a longitudinal sector from 140°E to 170°W, with maximum amplitude (averaged over the 0°–10°S latitude band) greater than 20 m s^{-1}. This strong westerly period constituted WWB2, which was the best defined WWB in COARE. ICE2 remained near the leading edge of the westerly region as it propagated eastward (Fig. 9b). WWB2 and ICE2 provide an excellent opportunity for case studies of the interaction between the convection and the wind field.

The IFA and LSA were suppressed for most of January (Fig. 9c), except for a short period of convective activity in the middle of the month (17–19 January, see Figs. 4a, 4b, and 6). The zonal winds in the COARE longitudes swung from westerly to easterly as ISO2 receded toward the east and ISO3 approached from the west. The ICE3 cloudiness seems to disappear near 130°E because it dropped south of the 0°–10°S latitude band displayed in Fig. 9c (see Figs. 8o and 8p). Despite this shortcoming of Fig. 9c, ICE3 did "jump" over the IFA (Figs. 8n–p). Anomalous low-level easterlies predominated along with a lack of deep convection in the IFA in January. Several large, relatively isolated, convective systems (developed within the ITCZ) propagated into the COARE domain from the northeast and some redeveloped within the LSA.

ICE3 became quasistationary over the western Pacific region near the date line in early February (Fig. 9d), and the LSA remained under the strong westerly regime (WWB3) to the west of ICE3. WWB3 and the deep convection actually shifted westward from 9 to 28 February (Fig. 9d) in the form of westward-propagating Rossby-wave-like disturbances in the wind field shown in Figs. 8r–s.

Especially striking in Fig. 9 are westward-propagating disturbances with a local periodicity of ~2 days (e.g., 9–19 December in Fig. 9b and 1–9 February in Fig. 9d). The 2-day disturbances occurred in all the ICEs (e.g., throughout all of December in Fig. 9b in ICE2 and from late January to late February in Fig. 9d). These disturbances gave rise to a ~2-day variability of IR temperatures in the time series over the IFA (Fig. 10).

Figure 10 illustrates the vertical structure of the ~2-day variation of total cloudiness. Contours are the percent area covered by infrared cloud-top temperatures in 5 K intervals over the IFA during the periods of 9–17 December and 20–28 December. Temperature axis is inverted to make it resemble a height coordinate. Eight well-defined events with a near 2-day period can be seen (i.e., 9, 11, 13, and 15 December in Fig. 10a and 20, 22, 24, and 26 December in Fig. 10b). Typically these systems began as a rapid development of very cold clouds. They subsequently weakened and left long-lasting large decaying (warmer) cloud shields, which persisted through the next day. The low-θ_e downdrafts produced by these large convective systems may prevent new convection from developing in the second day by "shutting off" the boundary layer. A slow boundary-layer recovery time (up to ~18 h) is observed by Parsons et al. (1994) in the wake of a convective system dur-

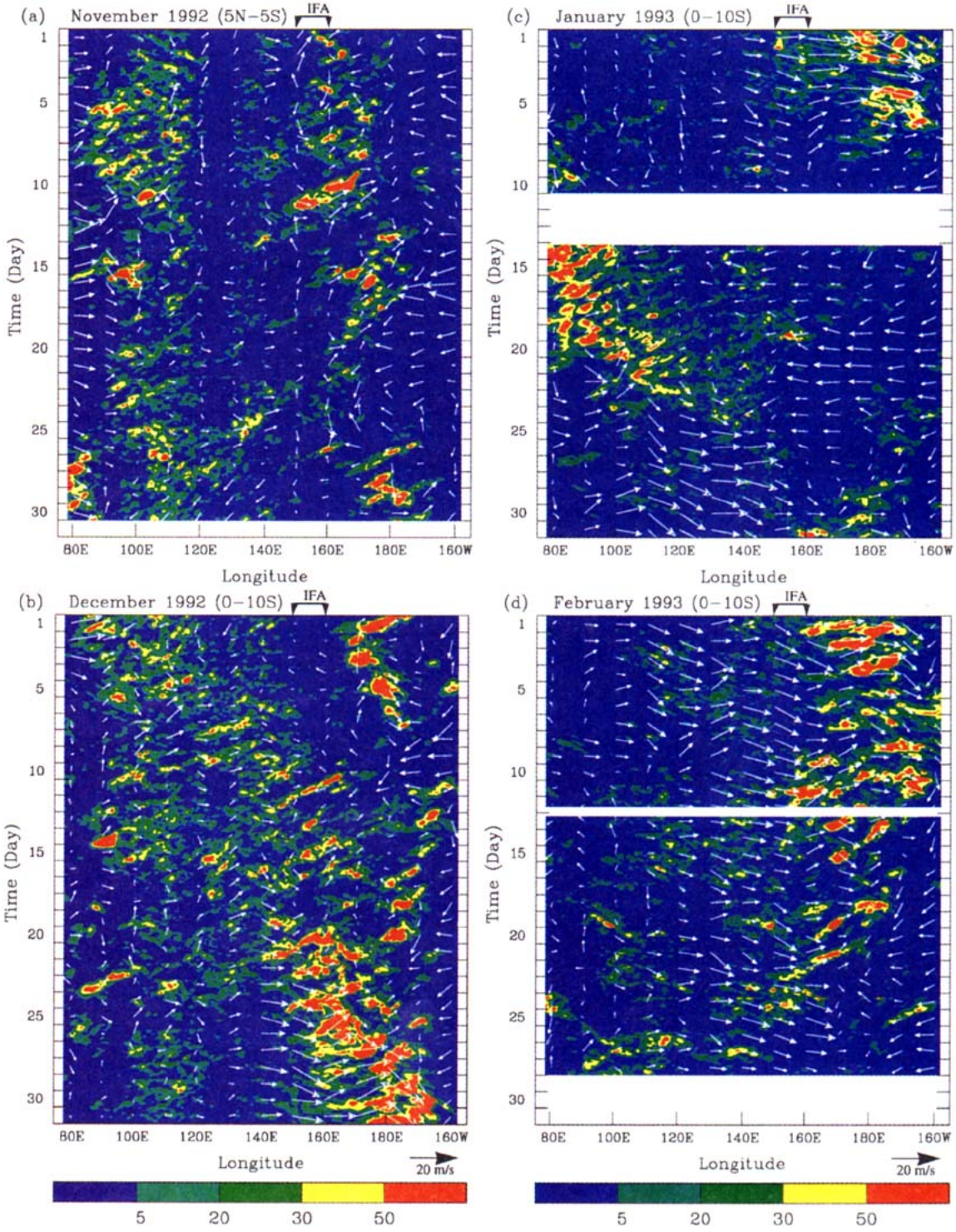

FIG. 9. (a)–(d) Time–longitude sections of deep convection with cloud-top temperature <208 K for each month from November 1992 to February 1993. The contours are the number of pixels colder than 208 K in a 10° latitude band at each longitude grid. The vectors are 850-mb total wind (m s^{-1}) averaged over the 10° latitude band. Position of the IFA is indicated at the top of the figures.

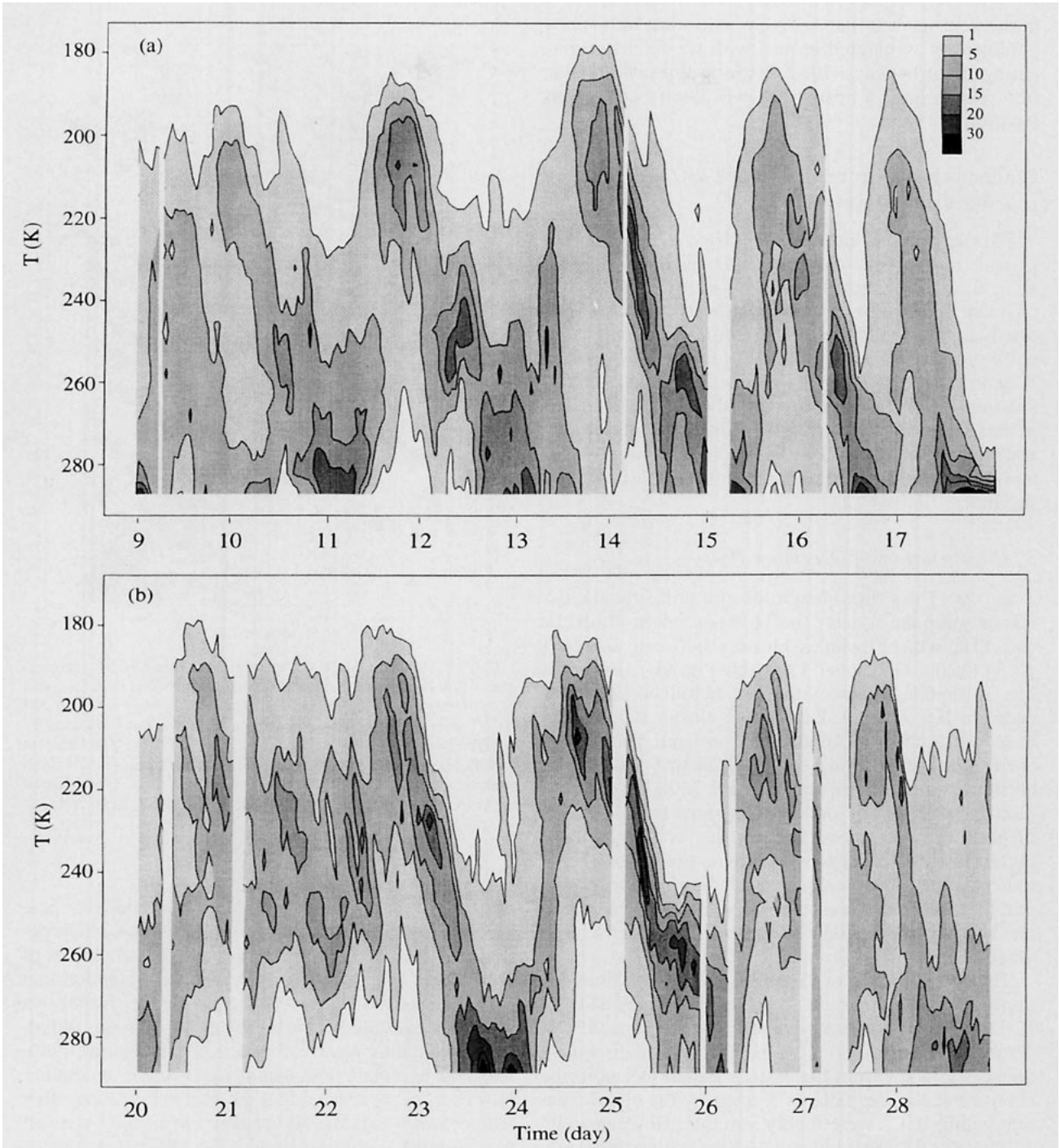

FIG. 10. Percent area (pixels) of cloud-top temperature within each 5 K interval over the IFA, (a) 9–17 December 1992 (UTC) and (b) 20–28 December 1992 (UTC). Contours are drawn at 1, 5, 10, 20, and 30% (per 5 K per hour). The date marker is at 0000 UTC (1100 LST).

ing COARE. The long-lasting, warmer cloud shields may have also partly contributed to the slow boundary-layer recovery by reducing the amount of solar heating that reaches the surface. If this were a purely local temporal oscillation, an explanation could be sought in the radiative effects of this long-lasting cloud coverage. But the consistent westward propagation of these 2-day cloud anomalies (seen in Fig. 9) suggests that the dynamics are probably important too (e.g., Takayabu 1994). We will present evidence

in the next section that the 2-day variation in IR temperatures is associated in part with westward propagating disturbances with a distinct diurnal modulation, which have a near 2-day periodicity at a given location.

5. Cloud clusters in relation to the ISO and 2-day disturbances

This section examines the cloud entities comprising the total cloudiness patterns seen in Figs. 2, 3, 8, and 9. The basic cloud entity in this discussion is the cloud cluster, which we have defined as a closed contour surrounding a spatially contiguous region of cloud-top temperature < 208 K in an IR satellite image (section 2b and d). In this section, we investigate how cloud clusters group together in time and space to produce the regions of anomalous high cloudiness associated with the ISO and 2-day disturbances noted at the end of the last section.

a. Cloud clusters of December 1992

Figure 11 is a time–longitude plot of all cloud clusters between the equator and 10°S (except in Figs. 11b and 11d, which includes clusters between 1°N and 10°S) during December 1992 (cf. Fig. 9b). Boxes in Fig. 11a indicate regions that are examined in greater detail in Figs. 11b–e. Each cloud cluster is indicated at the position of its centroid by an oval. The size of each oval is proportional to the actual size of the cloud cluster (cloud clusters smaller than 2000 km^2 are not plotted). Chains of cloud clusters show the life cycles of particular convective systems that consist of these cloud clusters. The east–west progression of the chains indicates the zonal component of their motions. Note that the zonal motion of these satellite-observed cloud clusters may differ from the motion of the intense convective components within each cloud cluster.

The general band of enhanced cloudiness from the upper left to lower right indicates the progression of ICE2, which became particularly intense after 20 December near 160°–180°E. As ICE2 migrated discontinuously eastward from the eastern Indian Ocean to the central Pacific, the patterns formed by the cloud clusters within ICE2 were highly variable. However, Fig. 11 reveals certain systematic features within this large-scale ensemble. The myriad of individual clusters in Fig. 11a was not a random distribution. Within the envelope of the ICE2, westward propagating streaks of the cloud clusters, with a periodicity of ~2 days, are apparent, especially during middle to late December. These wavelike disturbances consisted of *groups* of westward propagating (and some eastward-propagating) cloud clusters.

Figures 11b and 11c show that these disturbances propagated westward at 10–15 m s^{-1} over a zonal distance of 2000–4000 km. At a fixed longitude, the passage of these disturbances accounts for the 2-day periodicity of cloudiness noted in the spectral studies of Lau et al. (1991), Sui and Lau (1992), Hendon and Liebmann (1994), and Takayabu (1994). Nakazawa (1988) suggested that the westward propagating cloudiness anomalies were embedded in larger-scale intraseasonal eastward propagating convective anomalies. However, he postulated that the westward propagating feature was a single cloud cluster (or a single convective system). Figures 11b and 11c show that a westward propagating 2-day disturbance was typically made up of a fluctuating group of separate convective systems whose lifetimes were individually much less than the 2-day disturbance in which they occur. Cloud clusters within the 2-day disturbances went through sequential growth, splits, mergers, dissipation, and redevelopment within the same zonal disturbance with a horizontal scale of thousands of kilometers. This cloud-cluster ensemble structure of the westward propagating 2-day disturbances differs from Nakazawa's descrip-

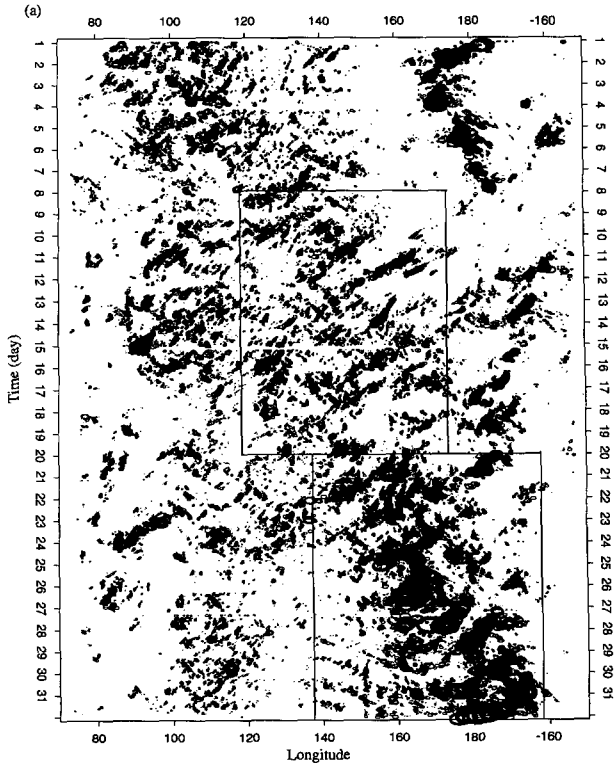

FIG. 11. Time–longitude diagrams of cloud clusters (IR temperature < 208 K) centered between 0° and 10°S (1°N and 10°S for b and d), (a) December 1992, (b) and (c) enhanced windows for 8–19 and 20–31 December, and (d)–(e) enhanced windows for 11–17 and 22–28 December. The date marker is at 0000 UTC (or 1100 LST at 156°E). Sizes of each oval are proportional to the sizes of actual cloud clusters. Arrows and numbers in (d) indicate the location and date of each aircraft mission during 12–15 December 1992. A, B, and C in (e) indicate three convective systems.

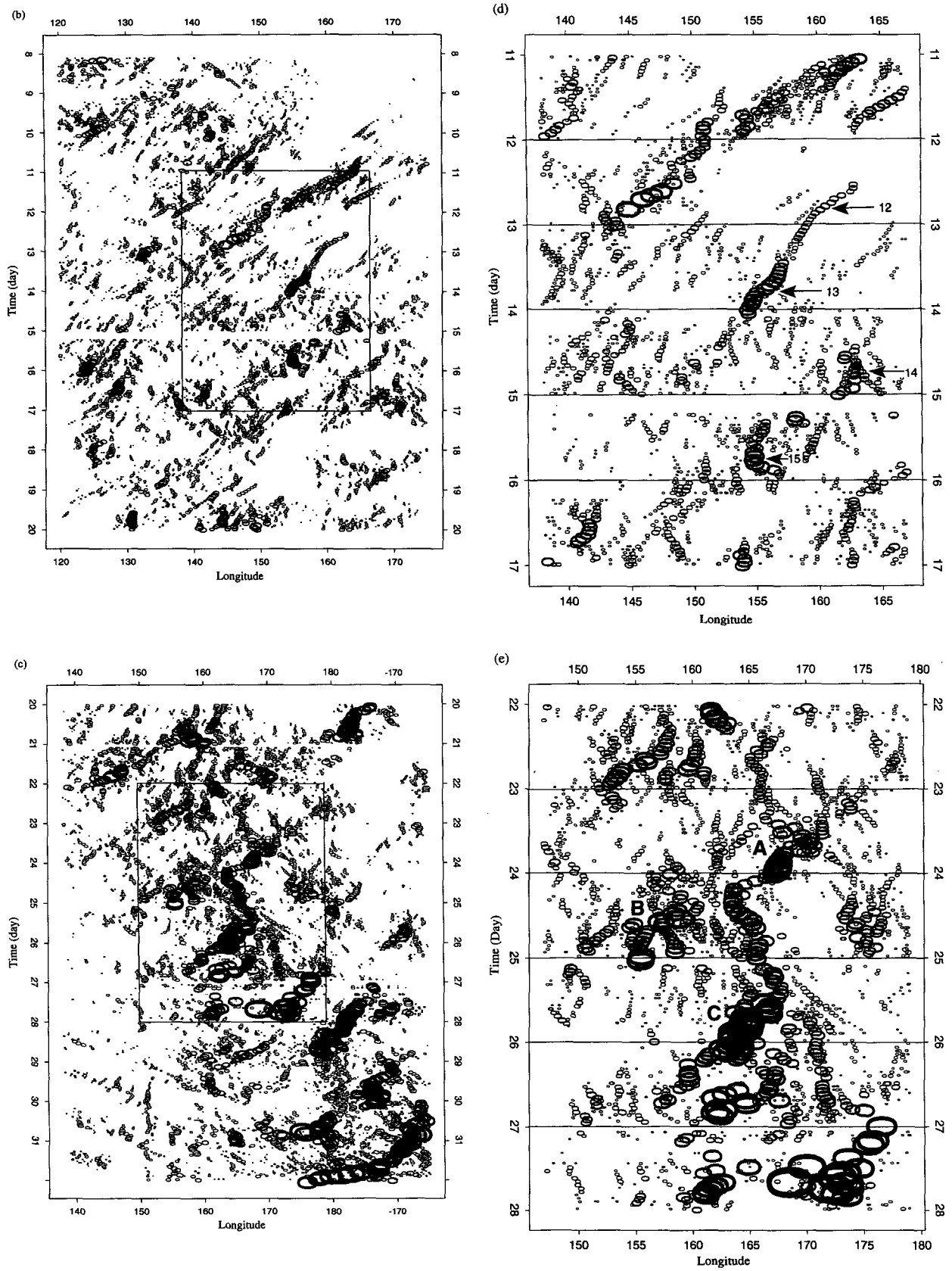

FIG. 11. (*Continued*)

tion of the streak of cold cloudiness as a single westward moving cluster.

Cloud clusters are highly intermittent in space and time and they are subject to diurnal variability (Fig. 7). Careful inspection of the GMS IR images and COARE aircraft and ship radar data indicates that the cloud clusters correspond to contiguous precipitation areas of 100–200 km^2 and were generally part (or a snapshot) of convective systems. The patterns are complicated by the fact that each individual convective system has a complex lifecycle, which involves some combination of movement, merging, splitting, strengthening, weakening, and dissipation. The behavior of individual convective systems is affected by environmental winds (e.g., LeMone et al. 1984; Rotunno et al. 1988), which were fluctuating locally, cold-pool dynamics (e.g., Zipser 1969) and other convective triggering mechanisms, gravity wave dynamics (Bretherton and Smolarkiewicz 1989; Mapes 1993), local distributions of atmospheric humidity and sea surface conditions, and other factors distinct from the dynamics of the 2-day disturbances in which the clusters were embedded.

Although the westward propagating disturbances flourished within ICEs, they were also evident at other times, for example, 10–11 November (150°–165°E, Fig. 9a). In December, 208 K cloudiness shows a similar 2-day interval east of the date line (Fig. 9b), which was not part of ICE2. This observation suggests that the westward propagating 2-day wave-like disturbances are not uniquely related to the intraseasonal oscillation.

b. *Cloud clusters during the onset of westerlies*

Figure 11b and its further enlargement Fig. 11d show that a series of westward propagating cloud clusters, or groups of cloud clusters, affected the COARE longitudes during mid-December in the early stage of the development of the intense convection and strong low-level westerlies of the December westerly wind burst over the COARE domain (Fig. 9b). Figure 11d indicates that, in some cases, the cloud clusters comprising the 2-day westward propagating disturbances moved at the same speed as the overall disturbance, while at other times the centroids of the cloud clusters were zonally stationary or even moved eastward (e.g., on 14 and 15 December). These observations suggest that the 2-day wave has an existence and intrinsic scale beyond its embedded deep convection structures or, in other words, that it contains a clear-air signal in addition to its convective cloudiness signal with comparable time and space scales for the cloudy and clear regions. Perhaps a very careful examination of thermodynamic data from this period could illuminate the mechanism of organization of the convection by the 2-day wave.

Three well-defined examples of the westward propagating 2-day disturbances occurred between 140° and 165°E (in the vicinity of the IFA) on 11–15 December. Four COARE aircraft missions sampled two of these disturbances. Arrows in Fig. 11d show the location of the aircraft at the approximate midtimes of the four flights. The flights were in four separated convective systems.

Figures 12a and 12b show both satellite and radar views of two of the cloud clusters sampled by the COARE aircraft. Airborne radar data obtained with the NOAA WP-3D aircraft lower-fuselage radar on 12 December (Fig. 12a) showed that the cloud cluster in Fig. 11d represented a typical large tropical oceanic cloud cluster (Houze and Betts 1981). This cloud cluster had a leading region of convective precipitation (more intense spots of echo on its southwest side in Fig. 12a) and a trailing region of stratiform precipitation (relatively uniform weak-moderate echoes on the northeast side in Fig. 12a). The leading-line–trailing-stratiform echo structure was maintained by discrete redevelopment, not continuous propagation. The 12 December system died during the time of the diurnal minimum in the early afternoon of 13 December. New convection broke out along a convective cloud line in the vicinity of the dissipated 12 December convective system and tracked slowly northwestward as it grew and intensified (Figs. 12a–b). The precipitation patterns of the 13 December system were more complex with multiple convective and stratiform regions (Fig. 12b). In both panels, the radar indicates large contiguous rain areas comparable to the $T < 208$ K areas, which are enhanced in red.

The cloud clusters in the next 2-day disturbance in the vicinity of the IFA (150°–165°E) on 14–15 December formed a very complex pattern in the time–longitude plot shown in Fig. 11d. Aircraft sampled two individual convective systems on 14–15 December (arrows in Fig. 11d), respectively. The cloud clusters on these two days did not form as a continuous pattern in time–longitude space as did the cloud clusters on 12–13 December.

The airborne radar data obtained on all four flights (12–15 December) repeatedly showed precipitation patterns typical of mesoscale precipitation features, as previously reported by Leary and Houze (1979) and many others. The mesoscale precipitation features were individually ~100–200 km in dimension. Often these mesoscale precipitation features were juxtaposed so closely that they combined to form contiguous or nearly contiguous precipitation over a region several hundred kilometers in dimension (Fig. 12b). In the cloud clusters observed by aircraft, the satellite-observed cloud shields with $T < 208$ K reached class 4 in size (Fig. 5) and corresponded closely to the large precipitation area formed by the juxtaposed mesoscale precipitation features. Two of the four convective systems (13 and 15 December) investigated by aircraft were class 4 in size. Note that even at this extreme size, these convective systems all had lifetimes of less than one day.

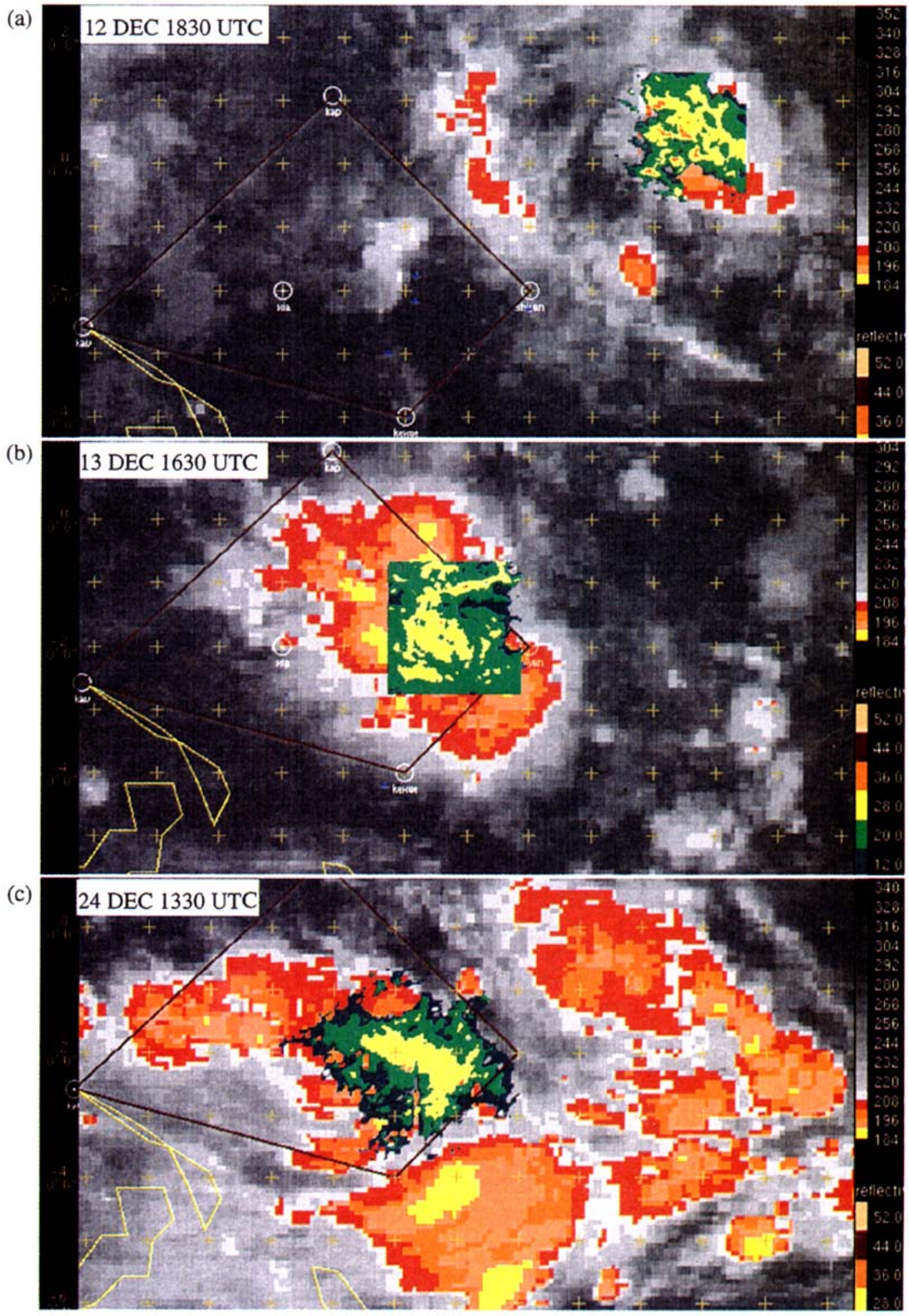

FIG. 12. NOAA WP-3D N43RF aircraft lower fuselage radar image overlaid on GMS IR images at (a) 1830 UTC 12 December 1992, (b) 1630 UTC 13 December 1992, and (c) MIT radar image from R/V *Vickers* overlaid with GMS IR image at 1330 UTC 24 December 1992. Both radars are C-band (5-cm wavelength). These images illustrate part of the precipitation region of cloud clusters shown in Figs. 11d and 11e. Color scales indicate radar reflectivity (dBZ) and IR temperatures (K). The COARE IFA is outlined.

The effect of the diurnal cycle on the cloud clusters is clearly evident. Each of the four aircraft-sampled convective systems died out during the time of the diurnal minimum (~0000–0300 UTC or 1100–1400 LST, see Fig. 7). Most of them were enhanced with a large areal extent at ~1800 UTC (0400 LST). Such diurnal behavior is found in almost all of the large convective systems.

c. *Cloud clusters during the westerly wind burst*

Figures 11c and 11e focus on the intense convection of late December. During this period, ICE2 became very intense and the lower-tropospheric westerlies spanned over 40° of longitude (Fig. 9b). The ovals making up ICE2 in Fig. 11c and 11e are larger and much more numerous than those in Fig. 11d. Despite the strong westerly flow, the chains of ovals in Figs. 11c and 11e indicate that a great many cloud clusters (more than 60%) tended to track westward, presumably by discrete propagation or successive redevelopment. Again, the diurnal effect is apparent, and the clusters are more pronounced around 1800 UTC (early morning) than at 0600 UTC (afternoon) on each day. Four 2-day westward-propagating disturbances (i.e., 21–22, 23–24, 25–26, and 27–28 December) were still evident, though less clear than those in Fig. 11d, during this period.

During the most convectively active period shown in Fig. 11e, the ovals representing cloud cluster centroids tend to jump around rather erratically (especially system B on 24 December). The reason is that as cloud clusters merge and split from one satellite image to the next, centroids can move discontinuously. This frequent merging and splitting is an early indication that the convection of late December was so active that the scale-separation between MCSs, with typical scales of ~100–200 km, and the larger scales (1000's of km) began to break down.

The horizontal structures of three convective systems A, B, and C (as indicated in Fig. 11e) are illustrated in Fig. 13, which shows satellite IR images every 6 hours (except panels a, b) for two days. The three convective systems were extremely large, tangled, and complex, and there is ambiguity about where one ended and the next began. The colder cloud tops suggest considerable substructure on the 100–200-km scale, the size of mesoscale precipitation features (Leary and Houze 1979). Figure 12c shows a radar echo in a portion of the convective system B, two hours after the time of Fig. 13c. It shows that a large contiguous region of precipitation underlay the region of cloud-top temperature < 208 K, extending to and presumably beyond the range of the MIT radar on R/V *Vickers*. Viewing of the ship radar data in time lapse reveals that convective system B contained several mesoscale precipitation features ~100–200 km in dimension. At some times these precipitation features were separated. At other times, they merged and interacted, like that shown in Fig. 12c. The rain area covered a region > 350 km in dimension, corresponding roughly to the region of IR temperature < 208 K. However, close inspection of sequences of radar images reveals that the ~100–200 km features were present as regions of higher reflectivity within the general large rain area.

The diurnal cycle of various cloud-top temperatures is well demonstrated in Fig. 13. There were many more large blue areas (220–235 K) than red (<208 K) during the local afternoon (Figs. 13b and 13f). The 208 K area was dominant during predawn hours (Figs. 13d and 13h). This behavior is consistent with Fig. 10, which shows that convective systems began as the expansion of very cold cloud tops in the first day (e.g., A in Fig. 13a and C in Figs. 13f–h) and weakened to become a large region of decaying warmer cloud tops (e.g., A and B in Figs. 13b and 13f) during the following afternoon. Convective system B developed 10° to the west of A (Fig. 13b) and intensified to maximum areal extent at the time of diurnal maximum in the early morning (Fig. 13d). Convective system C developed in a relatively clear region where convective system A was active two days earlier and dissipated near 168°E (Fig. 13b). Such behavior of convective systems was quite common within ICE2.

d. *Time clusters and superconvective systems (SCSs)*

To gain more insight into the organization of giant clusters and the characteristics of groups of cloud clusters within ICEs and the 2-day disturbances, we applied the tracking program of Williams and Houze (1987) to the four months of satellite IR data over the entire GMS domain. This program identifies and follows time clusters defined in section 2f. A time cluster is a set of cloud clusters (defined by the 208 K IR temperature threshold, section 2b) that exhibit time continuity through a series of satellite images. The criterion for time continuity was developed by Williams and Houze (1987) and retained by Mapes and Houze (1993). If the area of overlap of any two cloud clusters from one satellite image to the next (typically 1 hour apart) exceeds 5000 km^2, or if it exceeds 50% of the area of either cloud cluster, then the time continuity is established. Note that a time cluster may consist of one or more cloud clusters at a given time.

Figure 14 shows the lifetime versus the maximum size achieved by each time cluster during the COARE IOP over the entire GMS domain. The maximum size is expressed as a characteristic linear dimension (the square root of the area of IR temperature < 208 K cloud extent at the time of the maximum extent). Although maximum size is not very well correlated with lifetime, the likelihood that a time cluster will exceed a particular lifetime increases with increasing maximum time-cluster size (the upper limit of the point

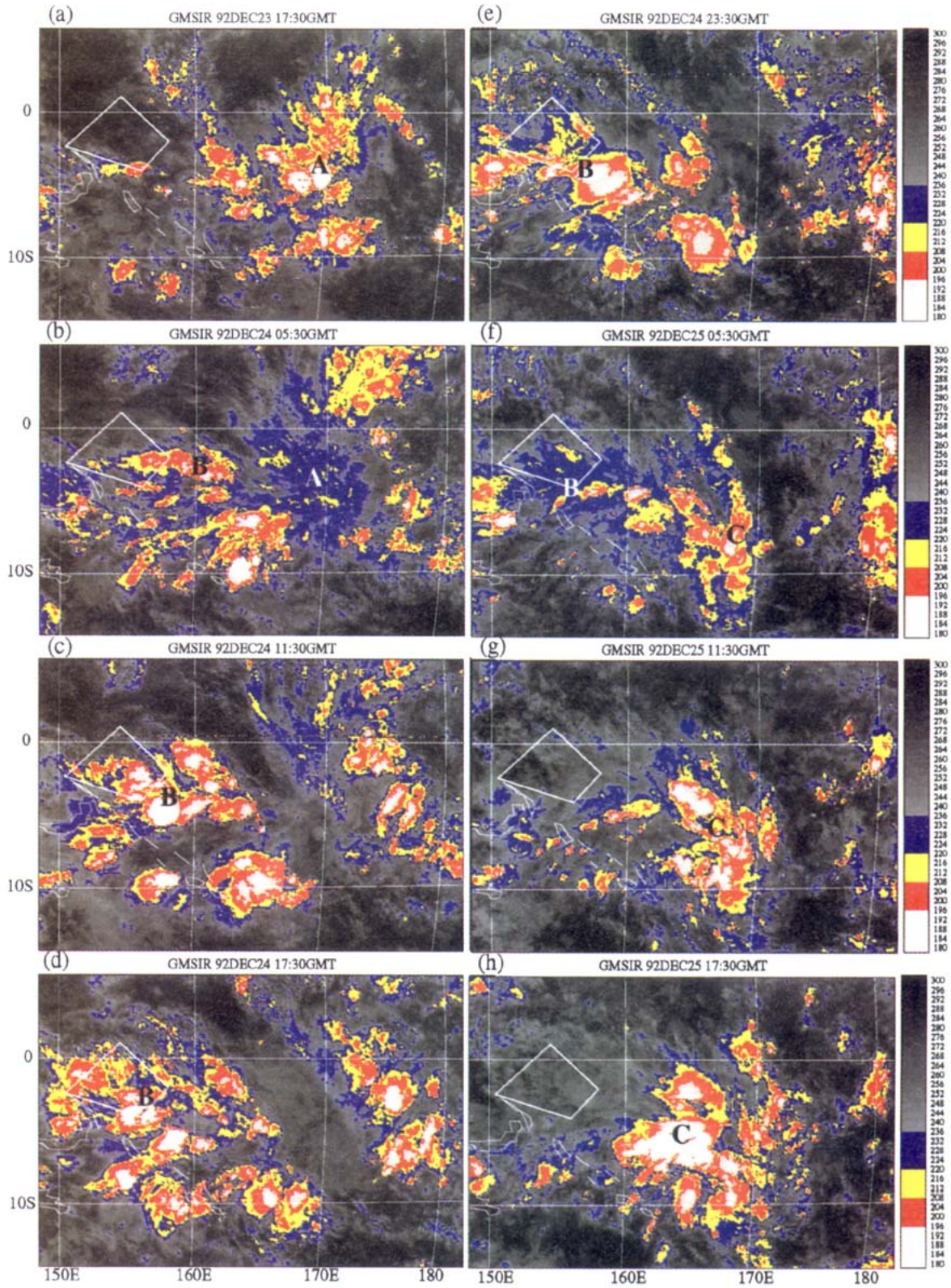

FIG. 13. GMS IR images [6-hourly, except for (a) and (b)] from 23–25 December 1992. A few key IR temperature ranges (K) are highlighted. A, B, and C indicate the locations of each convective system. The COARE IFA is outlined.

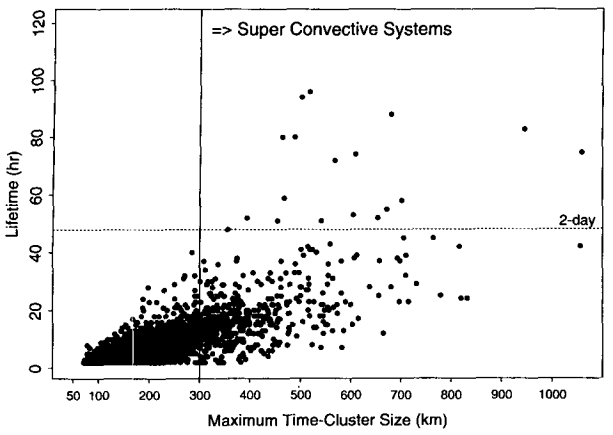

FIG. 14. Scatterplot of time cluster sizes versus lifetime over the warm pool (entire GMS domain in Fig. 2) during the COARE IOP. Each dot represents a particular time cluster with the maximum size reached during its lifetime.

spread in Fig. 14 increases more or less linearly with increasing maximum time-cluster size). Small, short-lived time clusters are the most numerous, but the few time clusters with very long duration and very large maximum size contain a sizable fraction of the total 208 K and colder cloud-top area. In particular, time clusters lasting over 48 hours (including five tropical cyclones) constituted some 15% of the total time cluster cloud coverage. Mapes and Houze (1993) termed these long-lived (>2 days) trackable entities *superclusters* (section 2f). Time clusters lasting over 24 hours constituted ~30% of the total time cluster cloud coverage. Note that small cloud clusters with the 208 K area less than 5000 km^2, which constituted about 20% of the total 208 K cloud coverage, are not included in the cloud coverage of the time clusters in Fig. 14.

Figure 14 includes many time clusters with a maximum size exceeding 300 km in dimension, which is the threshold that distinguishes the upper quartile (Class 4) of cloud clusters (Fig. 5). However, many of these large time clusters were of relatively short duration (12 hours or less). To describe these large time clusters, we define, without regard to duration, a superconvective system (SCS, section 2f) as any time cluster that achieves a maximum size > 300 km in dimension (right-hand portion of Fig. 14). This size criterion is the same as that used to define a class 4 cloud cluster (exceeding 9×10^4 km^2 in area, see Fig. 5). Note that every class 4 cluster (largest size quartile) is part of an SCS. The superclusters, which had lifetimes exceeding 2 days, were a subgroup of SCSs (upper right portion of Fig. 14).

Williams and Houze (1987) and Mapes and Houze (1993) have found that giant cloud clusters start to deviate from a lognormal distribution when they reach 300 km in dimension. The deviation from lognormality suggests that 300 km is the typical limit of the size of upper-level cloud tops of an individual cloud system (Lopéz 1977). A scale of 300 km is approximately the maximum horizontal distance that ice particles can travel from their convective-cell sources before falling out. SCSs whose maximum size exceed 300 km were invariably composed of multiple MCSs.

The cloud clusters within an SCS may either split from a common parent cluster or merge with each other during the lifetime of the SCS. However, an SCS can have a variety of structures and behaviors: it can be either a westward or eastward propagating time cluster, it may consist of one or several distinct cloud clusters, and its lifetime can be from several hours to a few days. These SCSs are best described by some examples from COARE.

e. Time clusters of December 1992

Figures 15a and 15b are time–longitude plots of time clusters (including only the cloud clusters > 5000 km^2 in area) for the same middle and late December periods examined in Figs. 11d and 11e within the same basic domains. The latitude band in Fig. 15a extends to 3°N in order to include the entire lifecycles of three large time clusters between 140°–165°E on 11–13 December. In Fig. 15, an oval is plotted at the centroid of all the cloud clusters making up a time cluster present at each hour. The size of the oval is the sum of the area covered by the member clusters of the time cluster at that time. Each oval thus represents an instantaneous time cluster. SCSs are labeled with a subscript according to the date of their initiation.

The overall westward propagation speed of the 2-day disturbances (identified in Fig. 11d, propagating from 165°E to 135°E during 11–17 December) is ~10–15 m s^{-1}. Figure 15a indicates that this mean motion consists of discrete regeneration of a new time cluster to the west (hundreds of km away) of the old time cluster during the daytime hours (diurnal minimum of $T < 208$ K area, see Fig. 7) and a nearly stationary or even eastward-moving centroid of the convective area during the night to dawn hours (diurnal maximum of $T < 208$ K area) in which the time cluster expands rapidly. This diurnal modulation is more apparent in Fig. 15a than Fig. 11d.

All three 2-day disturbances in Fig. 15a exhibit this diurnal behavior. Each of these 2-day disturbances consisted of a few SCSs plus many smaller time clusters. Within each of the 2-day disturbances, some of these SCSs (e.g., SCS_{10}, SCS_{11b}, and SCS_{13}) propagated westward up to 15 m s^{-1}, some were nearly stationary, while others moved slightly eastward (e.g., SCS_{11a}, SCS_{14}, SCS_{15}, and SCS_{16}) during the time of diurnal maximum of convective activity (1200–2000 UTC, i.e., night to dawn hours) when the cloud clusters within SCSs were expanding outward from the centroid in all directions. In almost all of these westward-propagating disturbances, SCSs were separated by the di-

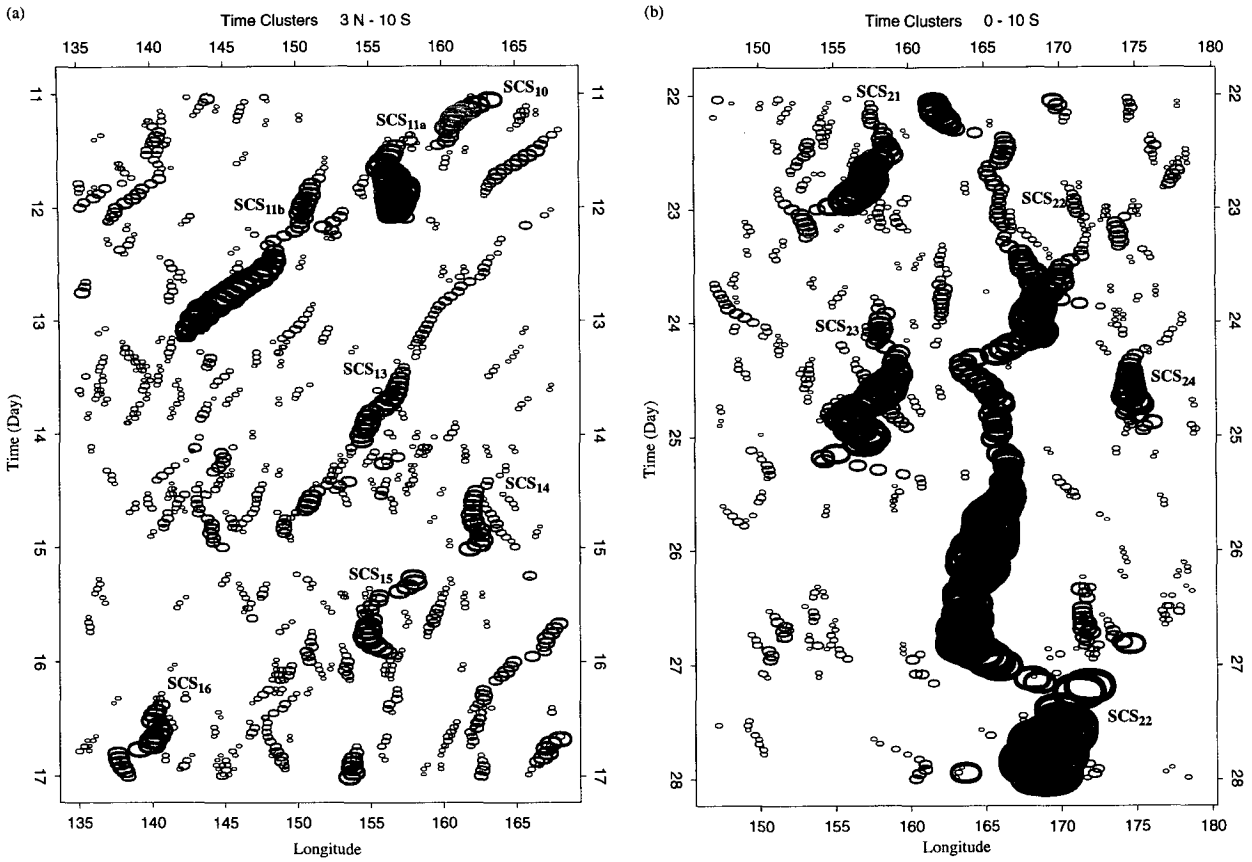

FIG. 15. Time clusters in time–longitude space for (a) 11–17 December 1992 and (b) 22–28 December 1992. Sizes of each oval are proportional to the sizes of actual time clusters at a given instant. SCSs indicate superconvective systems, and subscripts denote the starting date of each SCS.

urnal minimum of cold cloudiness in the daytime hours on each day.

Figure 15b shows a transition to a somewhat different behavior than that seen in Fig. 15a. During 22–24 December, the westward propagating 2-day disturbances were still evident. Four SCSs (SCS_{21}, SCS_{22}, SCS_{23}, and SCS_{24}) had a behavior similar to that seen in Fig. 15a. However, the size of these SCSs was visibly larger than those in Fig. 15a as the convective activity increased. During the most active phase of the ISO2, in late December, the cloud clusters were so numerous and overlapping that the tracking program tracked almost the entire ICE2 as a 5-day long supercluster. SCS_{22} reached its maximum area ($>1.2 \times 10^6$ km^2) on 28 December at 165°–175°E. This long-lasting eastward propagating time cluster satisfied the definition of a supercluster by the criteria of both Nakazawa (1988) and Mapes and Houze (1993). Between 25 and 28 December, the centroid of this supercluster drifted, somewhat erratically, eastward slowly at ~ 1 m s^{-1}, a typical speed for the ISO during its slow passage over the climatologically convective region of the western Pacific.

The observations presented here raise an important question. What is the natural scale of convective organization over the western Pacific warm pool? From the examinations of the satellite IR images at various resolutions, it is surprisingly difficult to say. One can identify individual precipitating convective cells in radar data (e.g., Fig. 12). However, attempts to follow such a cell through its lifecycle to obtain a description of the prototype member of the ensemble of cumulonimbus is almost impossible since initially well-defined cells and convective line segments eventually lose their identity and merge into larger, longer-lived mesoscale contiguous areas of precipitation. For this reason, convective meteorology in recent decades has come to consider mesoscale convective systems (MCSs, e.g., Houze 1993 and many others) as a fundamental unit of convective precipitation. The MCS consists of both convective and stratiform precipitation regions, but within these regions the identities of individual cells often get lost. One of the most important mechanisms in the MCS is the boundary-layer cold pool that is formed by the collective effects of convective downdrafts in an MCS. This cold pool triggers the devel-

opment of new convective cells at its edges, thus maintaining the continuity of the system.

The time cluster tracking technique is a similar attempt to follow a single MCS or SCS through its lifecycle in order to obtain a prototype for a statistical treatment of the ensemble of MCSs whose collective effects interact with some larger-scale disturbances such as the 2-day wave and the ISO. In some cases, the MCSs and SCSs can be distinguished from the large-scale disturbances (Fig. 15a) in which they are embedded. However, Fig. 15b suggests that, in some other situations, this effort can also fail. Initially distinct MCSs merge and split so freely that they lose their individual identities during the most convectively active period in late December. The organizing mechanism in these ensembles of cloud clusters remains substantially unknown but almost certainly involves more than the boundary-layer cold pool dynamics that organize convective cells into MCSs.

6. Conclusions

We have provided an overview of deep convection and large-scale flow over the eastern Indian Ocean and the western Pacific warm-pool region during TOGA COARE. Three episodes of the intraseasonal oscillation (ISO) were strong modulators of the frequency of deep convection in the COARE domain. The eastward-propagating ISO was superimposed on the seasonal cycle and interacted with other climatological features such as the ITCZ and the SPCZ over the western Pacific (Fig. 8). Within the envelope marking the convectively active phase of the ISO, cloud clusters were frequently organized into westward-propagating 2-day disturbances, with a strong diurnal signal superimposed on them. These multiscale characteristics of deep convection and its relation to the large-scale circulation, as well as some implications for further theoretical studies of tropical convection and equatorial waves, are summarized as follows.

1) Most of the deep convection in COARE occurred in three convectively active periods separated by two suppressed periods (Figs. 3, 4a, and 4b). The frequency of deep convection during the active phase of the ISO was nearly ten times that of the suppressed phase. During the suppressed phases of the ISO, the SST in the COARE IFA increased to a significantly higher value than in the active phases (Fig. 4g), as was the case for the boundary-layer integrated CAPE (Brown 1994; David Parsons, personal communication, 1995). The near absence of deep convection over a large portion of the tropical western Pacific (Figs. 8e, 8g, and 8l) sometimes lasted for as long as ten days or more (Figs. 4a and 4b). This is of particular concern regarding the assumption that is often made in theoretical and modeling studies: the Tropics is always in a state of convective quasi-equilibrium. Under this assumption, the convective instability is removed by deep convection continuously so that the tropical atmosphere remains in a nearly equilibrium state (very small changes in CAPE) on timescales longer than convective scale ($\sim$1 day or less). The validity of such assumptions clearly depends on the time and space scales of the phenomena being investigated. The suppressed convection periods, which lasted several days or more (much longer than the convective scale), are a subject of further investigation.

2) The anomalous cloudiness associated with the convectively active phases of the ISO coincided with (but led slightly) enhanced low-level equatorial westerlies (e.g., Figs. 3, 4a, 4d, 8j, 8n, 9b, 9d). Convection was, however, suppressed when anomalously strong equatorial low-level easterlies predominated over the west Pacific warm-pool region near the equator (Figs. 4a, 4f, 8n, 9c). This observation suggests that the occurrence of enhanced convection in the ISO cannot be explained solely in terms of increased low-level wind *speed,* which increases the heat fluxes from the ocean surface. Other factors, such as advection of cooler and drier boundary-layer air from the region of the equatorial eastern Pacific SST cold tongue, may explain the lack of deep convection in the anomalous low-level easterlies. This indicates that there may not be a simple relationship between low-level wind speed and deep convection on the ISO time and space scales.

3) Rossby-wave-like disturbances (cyclonic gyres straddling the equator) were commonly observed in connection with episodes of persistent enhanced convection over the eastern Indian and western Pacific Oceans, where the ISO cloud ensemble (ICE) was most prominent. A region of anomalous westerlies, termed as westerly wind burst (WWB), and enhanced convection tended to be located between the gyres. These Rossby-wave-like disturbances were important in explaining the high cloudiness patterns in COARE. When this type of disturbance forms, the eastward-propagating ICE retrogrades westward (e.g., late February, Figs. 8s and 9d). These gyres sometimes culminate in the development of tropical cyclones. Four such cyclones formed during COARE. Furthermore, in contrast to the theoretical explanation of the ISO based on the Kelvin wave dynamics, the observed WWBs and the most intense convection in COARE were usually not symmetric about the equator, suggesting substantial non-Kelvin components. This asymmetry of WWB can also induce a rather different oceanic dynamical response than those centered on the equator.

4) Within the active phase of the ISO, the convection was frequently concentrated into westward-propagating disturbances with a local periodicity of $\sim$2 days (Figs. 9 and 11). Each of the 2-day disturbances consisted of a number of time clusters, which are groups of cloud clusters that exhibited continuity in time and space (Figs. 11d and 15a). These westward-

propagating 2-day disturbances were not simply a footprint of a single cloud cluster, as suggested by Nakazawa (1988). Rather, it was an envelope of numerous cloud clusters and time clusters of various sizes, which usually have a lifetime shorter than 2 days. The observed spatial scale of these 2-day cloud cluster envelopes was ~2000 km, with an average westward propagation speed of 10–15 m s^{-1}. This mean motion often consists of discrete regeneration of a new time cluster to the west (hundreds of km away) of an old time cluster during the daytime hours (diurnal minimum of cold cloud-top area, see Fig. 7) and a nearly stationary or even eastward-moving centroid of the growing cloud clusters during the night to dawn hours (diurnal maximum of cold cloud-top area).

The observed 2-day disturbances have the characteristics of an atmospheric wave with an intrinsic scale beyond its embedded deep convection structures. It contains a clear-air signal in addition to its convective cloudiness signal with comparable time and space scales for the cloudy and clear regions. Takayabu (1994) also found a 2-day westward propagating peak in space–time spectra in the very cold clouds over the central Pacific region and identified this mode with westward propagating inertio–gravity waves. In a numerical modeling study, Yoshizaki (1991) showed that the eastward propagating inertio–gravity mode has a meridional structure much less favorable than the westward propagating inertio–gravity mode for organizing near-equatorial convection.

The dispersion relation derived from the linear shallow water equations (Matsuno 1966) predicts that equatorially trapped inertio-gravity waves with a 20 m s^{-1} phase speed should have a period of ~2 days. The *moist* atmospheric dynamics (Gill 1982) and mean flow structure may explain the slower phase speed in the observed 2-day disturbances if they were inertio-gravity waves. In addition, the diurnal cycle of convective systems (near stationary during the night to dawn hours) may have also contributed to the overall slower phase speed (Fig. 15a). Although the upward motion associated with the waves may not be strong enough to provide sufficient uplifting to trigger the convection, it may destabilize the lower troposphere to make it more favorable for convection. The relationship between convection and equatorial waves such as the 2-day westward propagating inertio–gravity waves is not well understood. It is nevertheless clear that the deep convective activity in the equatorial warm pool region is modulated strongly by the wavelike disturbances as shown in this study.

5) The eastward propagating ICE was made up of numerous cloud and time clusters that often grouped together on larger time and space scales. Most of the time clusters within an ICE are MCSs and SCSs (Figs. 11d, 11e, and 15). In some cases, the MCSs and SCSs can be distinguished from the large-scale disturbances (e.g., Fig. 15a) in which they are embedded. However, in the most convectively active period of the ISO (late December), cloud clusters became so large and numerous that, for a few days, the tracking program identified almost the entire ICE as a long-lasting, single trackable SCS or a supercluster (Fig. 15b). This observation indicates the lack of a distinct scale-separation between convection and large-scale disturbances during the most intense convective periods in COARE. It raises an important question concerning cumulus parameterizations in the current regional and global numerical models with various grid resolutions.

6) The diurnal cycle of large cloud clusters strongly affected the behavior of the large-scale cloud cluster ensemble in both intraseasonal and 2-day disturbances. Both the westward growth of a new cloud cluster within a 2-day wave and the eastward regeneration of another 2-day wave envelope within the ICE all appeared to be intermittent, partly as a result of the diurnal cycle of the cloud clusters (Figs. 11b–e, 13, and 15a). Such superimposition of the diurnal cycle of the large convective systems and the large-scale disturbances was disrupted by the land–sea circulation induced diurnal cycle over the regions of the maritime continent where the ICE usually appears to be weakened. The mechanism of the diurnal cycle of the convective systems over the open ocean and its implication to the ISO and 2-day disturbances will be examined extensively in a forthcoming paper (S. Chen and R. Houze Jr. 1996, manuscript submitted to *Quart. J. Roy. Meteor. Soc.*).

7) Large-scale environmental conditions were evidently crucial to promote (inhibit) convection during the active (suppressed) phase of the ISO. The vigorous grouping of cloud clusters in the ICE may be partly due to the "gregarious convection" effect (Mapes 1993), which predicts that new cloud clusters are favored in the vicinity of older cloud clusters, which tend to destabilize their surroundings. In addition, convectively generated cold pools trigger new convection in the immediate vicinity of older cloud clusters. However, the cloud clusters did not show this chain reaction effect in the suppressed phases of the ISO—class 3 and 4 cloud clusters were not absent during these periods, rather they were only infrequent (e.g., Fig. 9a). This result suggests that favorable large-scale environmental conditions are needed for the grouping effect of clusters.

The multiscale interactive processes among tropical deep convection, large-scale flow, moisture distributions in the troposphere and boundary layer, and conditions at the ocean surface were quite complex in COARE. The interaction between deep convection and the large-scale circulation (e.g., enhanced low-level westerlies, moistening of mid- to upper level by convection, Fig. 4) appears to have been a positive feedback process during the active phases of the ISO. Such positive feedback was apparently overwhelmed by the inhibition of deep convection in the suppressed phases

of the ISO. It may not be hard to postulate the positive feedback processes. Perhaps the key to understanding *intraseasonal variability* lies in an understanding of *why convection is so restricted in suppressed periods.* Even though bulk instability measures (e.g., CAPE) are maximum, even though surface wind speed can be substantial (easterlies in January), and even though SST is at its highest, convection does not form in a widespread way in suppressed periods. These interactive processes between convection and its tropical atmospheric and oceanic environments remain the subject of active investigation.

Acknowledgments. Special thanks to Chidong Zhang, Randy Brown, Petra Udelhofen, and Frank Marks for many helpful discussions and suggestions during this project. David Kingsmill, Sandy Yuter, Peggy LeMone, and Steve Esbensen commented on an early version of this manuscript; Michael McPhaden provided the TOGA TAO buoy data; Xin Lin and Richard Johnson produced Figs. 4c and 4d; Marc Michelsen and Scott Katz provided computer software support; G. C. Gudmundson edited the manuscript; and Kay Dewar assisted with graphics. Radar data was provided by NOAA/NSSL/MRD, NCAR/RDP, and the Department of Atmospheric Sciences at Colorado State University. This research was supported by the National Science Foundation under Grant ATM-9024431, the Office of Naval Research under Grant ONR N00014-93-1-1271, the National Aeronautics and Space Administration under Grants NAG5-1599 (TRMM) and NAGW-2633 (EOS), the National Oceanic and Atmospheric Administration under Cooperative Agreement NA37RJ0198 (contribution number 314), and by the TOGA COARE International Project Office.

REFERENCES

Arkin, P. A., and B. N. Meisner, 1987: The relationship between large-scale convective rainfall and cold cloud over the western hemisphere during 1982–1984. *Mon. Wea. Rev.*, **115,** 51–74.

Bladé, I., and D. L. Hartmann, 1993: Tropical intraseasonal oscillations in a simple nonlinear model. *J. Atmos. Sci.*, **50,** 2922–2939.

Bretherton, C. S., and P. K. Smolarkiewicz, 1989: Gravity waves, compensating subsidence and detrainment around cumulus clouds. *J. Atmos. Sci.*, **46,** 740–759.

Brown, R. G., 1994: A modeling and observational study of convective interaction with large-scale dynamics in the Tropics. PhD. thesis, University of Washington, 193 pp.

Chang, C.-P., 1970: Westward propagating cloud patterns in the tropical Pacific as seen from time composite satellite photographs. *J. Atmos. Sci.*, **27,** 133–138.

——, and K. G. Lum, 1985: Tropical–midlatitude interactions over Asia and the western Pacific Ocean during the 1983/84 northern winter. *Mon. Wea. Rev.*, **113,** 1345–1358.

Charney, J. G., and A. Eliassen, 1964: On the growth of the hurricane depression. *J. Atmos. Sci.*, **21,** 68–75.

Chen, S. S., 1993: Equatorial westerly wind bursts and double cyclones. Preprints, *20th Conf. on Hurricanes and Tropical Meteorology,* San Antonio, TX, Amer. Meteor. Soc., 615–617.

——, R. A. Houze Jr., B. E. Mapes, S. R. Brodzik, and S. E. Yuter, 1995: TOGA COARE satellite data summaries available on the World Wide Web. *Bull. Amer. Meteor. Soc.*, **76,** 329–333.

Emanuel, K. A., 1987: An air–sea interaction model of intraseasonal oscillations in the Tropics. *J. Atmos. Sci.*, **44,** 2324–2340.

Gill, A. E., 1982: Studies of moisture effects in simple atmospheric models: The stable case. *Geophys. Astrophys. Fluid Dyn.*, **19,** 119–152.

Gutzler, D. S., G. N. Kiladis, G. A. Meehl, K. M. Weickmann, and M. Wheeler, 1994: The global climate of December 1992–February 1993. Part II: Large-scale variability across the tropical western Pacific during TOGA COARE. *J. Climate,* **7,** 1606–1622.

Hendon, H. H., and B. Liebmann, 1990: A composite study of the onset of the Australian summer monsoon. *J. Atmos. Sci.*, **47,** 2227–2240.

——, and ——, 1994: Organization of convection within the Madden–Julian oscillation. *J. Geophys. Res.*, **99,** 8073–8083.

——, and M. L. Salby, 1994: The lifecycle of the Madden–Julian oscillation. *J. Atmos. Sci.*, **51,** 2225–2237.

Houze, R. A., Jr., 1993: *Cloud Dynamics.* Academic Press, 573 pp.

——, and A. K. Betts, 1981: Convection in GATE. *Rev. Geophys. Space Phys.*, **19,** 541–576.

Hu, Q., and D. A. Randall, 1994: Low-frequency oscillations in radiative-convective systems. *J. Atmos. Sci.*, **51,** 1089–1099.

Keen, R. A., 1987: Equatorial westerlies and southern oscillation. *Proc. U.S. TOGA Western Pacific Air–Sea Interaction Workshop,* Honolulu, HI, UCAR, 121–140.

Knutson, T. R., and K. M. Weickmann, 1987: 30–60-day atmospheric oscillations: Composite life cycles of convection and circulation anomalies. *Mon. Wea. Rev.*, **115,** 1407–1436.

Lau, K.-M., 1982: Equatorial response to northeasterly cold surge as inferred from satellite cloud imagery. *Mon. Wea. Rev.*, **110,** 1306–1313.

——, and P. H. Chan, 1985: Aspects of 40–50-day oscillation during the northern winter as inferred from outgoing longwave radiation. *Mon. Wea. Rev.*, **113,** 1889–1909.

——, and S. Shen, 1988: On the dynamics of intraseasonal oscillations and ENSO. *J. Atmos. Sci.*, **45,** 1781–1797.

——, L. Peng, C.-H. Sui, and T. Nakazawa, 1989: Dynamics of super cloud clusters, westerly wind burst, 30–60 day oscillation, and ENSO: A unified view. *J. Meteor. Soc. Japan,* **67,** 205–219.

——, T. Nakazawa, and C.-H. Sui, 1991: Observations of cloud cluster hierarchies over the tropical western Pacific. *J. Geophys. Res.*, **96,** 3197–3208.

Leary, C., and R. A. Houze Jr., 1979: The structure and evolution of convection in a tropical cloud cluster. *J. Atmos. Sci.*, **36,** 437–457.

LeMone, M. A., G. M. Barnes, and E. J. Zipser, 1984: Momentum flux by lines of cumulonimbus over the tropical oceans. *J. Atmos. Sci.*, **41,** 1914–1932.

Liebmann, B., and H. H. Hendon, 1990: Synoptic-scale disturbances near the equator. *J. Atmos. Sci.*, **47,** 1463–1479.

Lin, X., and R. H. Johnson, 1996: Kinematic and thermodynamic characteristics of the flow over the western Pacific warm pool during TOGA COARE. *J. Atmos. Sci.*, **53,** 695–715.

Liu, G., J. A. Curry, and R.-S. Shen, 1995: Classification of clouds over the western equatorial Pacific using combined infrared and microwave satellite data. *J. Geophys. Res.*, **100,** 13 811–13 826.

Lopéz, R. E., 1977: The lognormal distribution and cumulus cloud populations. *Mon. Wea. Rev.*, **105,** 865–872.

Machado, L. A. T., M. Desbois, and C.-P. Duvel, 1992: Structural characteristics of deep convective systems over tropical Africa and the Atlantic Ocean. *Mon. Wea. Rev.*, **120,** 392–406.

Madden, R., and P. Julian, 1971: Detection of a 40–50 day oscillation in the zonal wind in the tropical Pacific. *J. Atmos. Sci.*, **28,** 702–708.

——, and ——, 1972: Description of global scale circulation cells in the Tropics with a 40–50-day period. *J. Atmos. Sci.*, **29,** 1109–1123.

——, and ——, 1994: Observations of the 40–50-day tropical oscillation—A review. *Mon. Wea. Rev.*, **122,** 814–837.

Mapes, B. E., 1993: Gregarious tropical convection. *J. Atmos. Sci.*, **50,** 2026–2037.

——, and R. A. Houze Jr., 1993: Cloud clusters and superclusters over the oceanic warm pool. *Mon. Wea. Rev.*, **121,** 1398–1415.

Martin, D. W., and A. J. Schreiner, 1981: Characteristics of West African and East Atlantic cloud clusters: A Survey of GATE. *Mon. Wea. Rev.*, **109,** 1671–1688.

Matsuno, T., 1966: Quasi-geostrophic motions in the equatorial area. *J. Meteor. Soc. Japan,* **44,** 25–43.

McPhaden, M. J., 1993: TOGA-TAO and the 1991–1993 El Niño–Southern Oscillation event. *Oceanogr.*, **6,** 36–44.

Murakami, T., and W. L. Sumathipala, 1989: Westerly bursts during the 1982/83 ENSO. *J. Climate,* **2,** 71–85.

Nakazawa, T., 1988: Tropical super clusters within intraseasonal variations over the western Pacific. *J. Meteor. Soc. Japan,* **66,** 823–839.

Neelin, J. D., I. M. Held, and K. H. Cook, 1987: Evaporation–wind feedback and low-frequency variability in the tropical atmosphere. *J. Atmos. Sci.,* **44,** 2341–2348.

Nitta, T., and T. Motoki, 1987: Abrupt enhancement of convective activity and low level westerly wind burst during the onset phase of 1986–87 El Niño. *J. Meteor. Soc. Japan,* **65,** 497–506.

Parsons, D., W. Dabberdt, H. Cole, T. Hock, C. Martin, A. Barrett, E. Miller, M. Spowart, M. Howard, W. Ecklund, D. Carter, K. Gage, and J. Wilson, 1994: The integrated sounding system: Description and preliminary observations from TOGA COARE. *Bull. Amer. Meteor. Soc.*, **75,** 553–567.

Ramage, C. S., 1971: *Monsoon Meteorology.* Academic Press, 296 pp.

Raymond, D. J., 1994: Convective processes and tropical atmospheric circulations. *Quart. J. Roy. Meteor. Soc.,* **120,** 1431–1455.

Reed, R., and E. Recker, 1971: Structure and properties of synoptic-scale wave disturbances in the equatorial western Pacific. *J. Atmos. Sci.,* **28,** 1117–1133.

Rotunno, R., J. B. Klemp, and M. L. Weisman, 1988: A theory for strong, long-lived squall lines. *J. Atmos. Sci.,* **45,** 463–485.

Rui, H., and B. Wang, 1990: Synoptic climatology of transient tropical intraseasonal convective anomalies. *Meteor. Atmos. Phys.,* **44,** 43–61.

Salby, M. L., R. R. Garcia, and H. H. Hendon, 1994: Intraseasonal behavior of clouds, temperature, and motion in the Tropics. *J. Atmos. Sci.,* **51,** 2344–2367.

Spencer, R. W., 1993: Global oceanic precipitation from the MSU during 1979–1991 and comparisons to other climatologies. *J. Climate,* **6,** 1301–1326.

Sui, C.-H., and K.-M. Lau, 1992: Multiscale phenomena in the tropical atmosphere over the western Pacific. *Mon. Wea. Rev.*, **120,** 407–430.

Takayabu, Y. N., 1994: Large-scale cloud disturbances associated with equatorial waves. Part II: Westward-propagating inertio–gravity waves. *J. Meteor. Soc. Japan,* **72,** 451–465.

Wallace, J. M., and V. E. Kousky, 1968: Observational evidence of Kelvin waves in the tropical stratosphere. *J. Atmos. Sci.,* **25,** 900–907.

Wang, B., 1988: Dynamics of the tropical low-frequency waves: An analysis of the moist Kelvin wave. *J. Atmos. Sci.,* **45,** 2051–2065.

Webster, P. J., and R. Lukas, 1992: TOGA COARE: The coupled ocean–atmosphere response experiment. *Bull. Amer. Meteor. Soc.,* **73,** 1377–1416.

Williams, M., and R. A. Houze Jr., 1987: Satellite-observed characteristics of winter monsoon cloud clusters. *Mon. Wea. Rev.*, **115,** 505–519.

Wyrtki, K., 1975: El Niño—The dynamic response of the equatorial Pacific Ocean to atmospheric forcing. *J. Phys. Oceanogr.,* **5,** 572–582.

Yoshizaki, M., 1991: On the selection of eastward-propagating modes appearing in the wave-CISK model as tropical intraseasonal (30–60 day) oscillations. Linear response to localized heating moving in an east–west direction on the equatorial beta plane. *J. Meteor. Soc. Japan,* **69,** 595–608.

Zangvil, A., and M. Yanai, 1981: Upper tropospheric waves in the Tropics. Part II: Association with clouds in the wavenumber-frequency domain. *J. Atmos. Sci.,* **38,** 939–953.

Zhang, C. D., 1996: Atmospheric intraseasonal variability at the surface in the tropical western Pacific Ocean. *J. Atmos. Sci.,* **53,** 739–758.

Zipser, E. J., 1969: The role of organized unsaturated convective downdrafts in the structure and rapid decay of an equatorial disturbance. *J. Appl. Meteor.,* **8,** 799–814.